AD-A139 550 INTERACTION OF A TURBULENT BOUNDARY LAYER WITH A NORMAL 1/1
SHOCK WAVE FOLLOW..(U) AERONAUTICAL RESEARCH LABS
MELBOURNE (AUSTRALIA) W H SCHOFIELD APR 83
UNCLASSIFIED ARL/MECH-ENG-161 F/G 20/4 NL

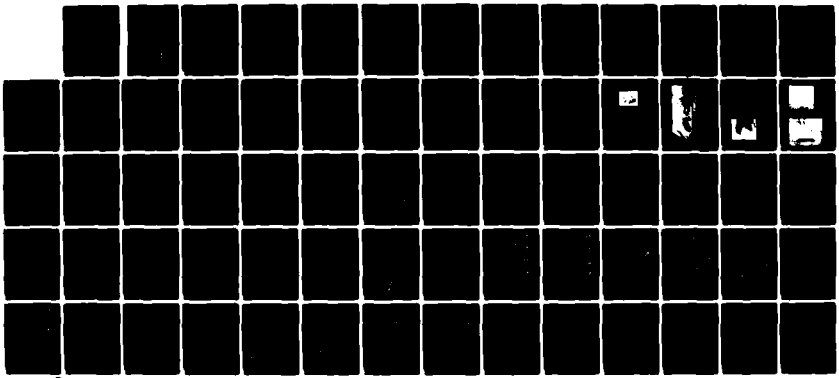

END
DATE FILMED
5-84
DTIC

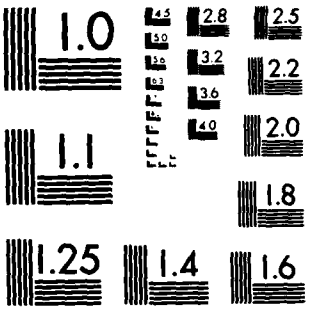

MICROCOPY RESOLUTION TEST CHART
NATIONAL BUREAU OF STANDARDS-1963-A

ARL-MECH-ENG-REPORT-161

AR-002-950

(12)

DEPARTMENT OF DEFENCE

DEFENCE SCIENCE AND TECHNOLOGY ORGANISATION

AERONAUTICAL RESEARCH LABORATORIES

MELBOURNE, VICTORIA

MECHANICAL ENGINEERING REPORT 161

INTERACTION OF A TURBULENT BOUNDARY LAYER WITH A NORMAL SHOCK WAVE FOLLOWED BY AN ADVERSE PRESSURE GRADIENT

by

W. H. SCHOFIELD

Approved for Public Release

COPY No

APRIL 1983

AR-002-950

DEPARTMENT OF DEFENCE
DEFENCE SCIENCE AND TECHNOLOGY ORGANISATION
AERONAUTICAL RESEARCH LABORATORIES

MECHANICAL ENGINEERING REPORT 161

INTERACTION OF A TURBULENT BOUNDARY LAYER WITH A NORMAL SHOCK WAVE FOLLOWED BY AN ADVERSE PRESSURE GRADIENT

by

W. H. SCHOFIELD

SUMMARY

An experimental study has been made of the development of a turbulent boundary layer after an interaction with a normal shock wave (strong enough to cause a local separation) in a strong adverse pressure gradient. This type of flow occurs in air breathing engine components (e.g. supersonic intakes, transonic compressor stages and supersonic diffusers), is poorly understood and cannot be satisfactorily predicted. The measurements, made in a closed duct, extended well downstream of the shock wave interaction. Detailed results for the flow are presented and used to support two major conclusions. Firstly it is shown that the post shock adverse pressure gradient has a large effect on boundary layer development through the interaction and downstream of it. Consequently existing results for interactions without a post shock pressure gradient should not be used as a model for practical flows which typically have strong pressure gradients applied downstream of the shock wave. The second conclusion was that the shock wave in a rectangular duct produced a pronounced stabilising effect on the downstream flow. Surface flow visualization suggests that this stabilization is achieved by streamwise vortices shed into the flow from the separated region formed by the shock wave. The implications of this result to nominally two-dimensional flow situations and to flows with weak interactions without local separations, is discussed.

POSTAL ADDRESS: Director, Aeronautical Research Laboratories,
Box 4331, P.O., Melbourne, Victoria, 3001, Australia

CONTENTS

NOTATION

Symbol	*Definition*
A	constant in logarithmic law of the wall ($= 5{\cdot}0$)
C_p	pressure coefficient referred to nozzle exit conditions
c_f'	skin friction coefficient ($= \tau_0/\frac{1}{2}\rho U_1^2$)
G	Clauser's shape parameter $\left(= \int_0^1 \left(\frac{u-U_1}{u_\tau}\right)^2 d\left(\frac{y}{\delta}\right)\right)$
H	form factor (δ^*/θ)
M	Mach number
M_1	local free stream Mach number
Pr	molecular Prandtl number
p_s	static pressure
p_w	wall pressure
P_T	total pressure
P_{TO}	total settling chamber pressure
Re_s	Reynolds number at shock wave position
T_w	wall temperature
T_o	local stagnation temperature
T_{oo}	settling chamber stagnation temperature
T_{o1}	free stream stagnation temperature
T_p	stagnation temperature measured by probe in the boundary layer
$\bar{T}$	$(T_p-T_w)/(T_{o1}-T_w)$
u	mean velocity in x direction
U_1	free stream velocity
$\bar{U}$	u/U_1
u_τ	velocity scale based on wall shear stress ($=(\tau_0/\rho)^{\frac{1}{2}}$)
x	distance from leading edge of duct floor
X	distance from start of wall pressure rise
y	vertical distance from the wall
δ	velocity boundary layer total thickness
δ^*	velocity boundary layer displacement thickness $\left(\approx \int_0^1 \left(1 - \frac{\rho u}{\rho_1 U_1}\right) d\left(\frac{y}{\delta}\right)\right)$
δ_u^*	displacement thickness immediately before the shock wave or pressure rise
δ_I^*	displacement thickness at start of mixing region
ϵ	normalised enthalpy thickness $\left(= \int_0^1 \left(\frac{\rho u T_p}{\rho_1 U_1 T_{o1}} - 1\right) d\left(\frac{y}{\delta}\right)\right)$

κ	Karman constant (0·40)
Π	Coles' wake strength parameter
ρ	fluid density
ρ_1	free stream fluid density
θ	boundary layer momentum thickness $\left(= \int_0^1 \frac{\rho u}{\rho_1 U_1}\left(1 - \frac{\rho u}{\rho_1 U_1}\right) d\left(\frac{y}{\delta}\right)\right)$
τ_0	wall shearing stress
ψ	stream function

1. INTRODUCTION

This report presents measurements of boundary layer development in a strong adverse pressure gradient after an interaction with a normal shock wave strong enough to cause a local separation in the boundary layer. This type of flow occurs in several important practical situations such as: supersonic intakes (Stewart & Fisher (1970)), transonic compressor stages (Leblanc & Goethals (1975)), supersonic diffusers (Seddon (1967)) and also on transonic aerofoils (Vidal, Wittliff, Catlin & Sheen (1973), Vidal & Catlin (1977), Inger & Mason (1975), Alstatt (1977), Vidal & Kooi (1976), Alber, Bacon, Masson & Collins (1973)). It is very poorly predicted by current calculation methods (Vidal & Kooi (1976)).

It would have been satisfying to devise an experiment that was relevant to all these flows. However, the present experiment achieved this aim to only a limited extent. Firstly the influence of three dimensional effects will probably be quite different in the various flows. The experimental layer which was studied developed on the floor of a rectangular duct and therefore the results will be more relevant to a rectangular supersonic intake than for example a transonic aerofoil. Secondly, the experiment involved a boundary layer developing on a flat plate in zero pressure gradient before interacting with a normal shock wave, whereas flow on transonic aerofoils, in supersonic diffusers and transonic compressors have a favourable pressure gradient before the shock wave, and some supersonic intakes have adverse pressure gradients before the shock wave. This is not, however, thought to be an important difference, because of the overwhelming changes to a boundary layer brought about by impulsive separation at a shock wave and the vigorous mixing which precedes reattachment. Given this dominating influence of the shock wave on the layer's behaviour, the initial condition of the layer entering the interaction will have a negligible effect on its downstream development. Differences in upstream conditions will cause layers of different thicknesses to be generated before the shock wave, but this just means an increase in the size but not the structure of the interaction and apparently does not, affect the layer's downstream behaviour (Little (1967), Vidal & Kooi (1976)). Therefore the absence of pressure gradient before the shock wave is argued to have little effect on the generality of these results.

Previous work on the problem has been of three types. Firstly there have been engineering studies with the aim of improving the performance of a particular piece of hardware (e.g. Brown, Nawrocki & Paley (1968)). Secondly there have been several studies of normal shock wave–boundary layer interaction with no (other) pressure gradients applied to the flow (Seddon (1967), Kooi (1975), Matear, Bresh & Viegas (1976), East (1976), Sawyer, East & Nash (1977), Abbiss, East, Nash, Parker, Pike & Sawyer (1976)). Finally in two cases (Vidal *et al.* (1973), Padova, Falk & Wittliff (1980)) flows with limited post-shock pressure gradients have been generated in blowdown Ludwieg tubes by varying the porosity of a perforated nozzle. However the pressure gradients have been mild and their effect observed over a very short distance downstream of the shock wave.

There exist therefore, experimental data on the effect on boundary layer development of a normal shock wave without an adverse pressure gradient and of course there exist numerous studies of subsonic turbulent boundary layer development in strong adverse pressure gradients (see Coles & Hirst (1968)). In the absence of data on the combined effect of the two agencies it is tempting (see Inger (1975)) to add these two separate effects to estimate boundary layer development in an adverse pressure gradient after an interaction with a normal shock wave. However as turbulent boundary layers are highly non-linear a simple addition is probably incorrect. It is a question addressed in this study and is of theoretical as well as practical interest. The theoretical interest arises from the technique of studying the turbulent mechanisms within a turbulent boundary layer by analysing the response of a layer to discontinuous or step changes in boundary conditions (see Clauser (1956)). A normal shock wave impinging on a zero pressure gradient boundary layer can be considered as impulsively applying a pressure step to the layer.

Seddon (1967) observed the layer's response to such an impulse for a distance of fifty (undisturbed) layer thicknesses which is further than any other worker has done. His results showed that the effects of the shock wave on the layer were still evident at the last observation station. In his flow there was no pressure gradient applied after the shock wave and it may be that the response took a long time to die out as it was simply decaying in the absence of other strong forces. It is possible in the flow studied here that the strong post shock pressure gradient will dominate the flow and quickly erase the effects of the shock wave. To separate the effects of shock wave and pressure gradient we require reference or comparison layers that have one of the agencies (shock wave or pressure gradient) absent but otherwise are identical to the main flow under investigation. In the present study, therefore, results were taken in a reference layer that developed in the same adverse pressure gradient as the main flow but without the shock wave. Results by Seddon (1967)[1] provide the other reference layer with a normal shock wave but no post shock adverse pressure gradient. With these three sets of results the effect on boundary layer development of shock wave, pressure gradient and their combination can be evaluated.

2. EXPERIMENT

2.1 Experimental Rig

The experimental rig is shown diagrammatically in figure 1. An undried air supply of 4·26 kg/s was heated to a stagnation temperature of 403K (to prevent subsequent condensation shocks) and passed into a settling chamber of 0·605 m diameter containing six wire screens. The flow area was then reduced subsonically in a duct section that changed from circular to rectangular. The area reduction ratio from the settling chamber to the sonic throat was 40 to 1 (details are given in Schofield (1975)). The flow was then accelerated to Mach 1·41* giving an exit static temperature near ambient. Mach 1·41 was chosen as being representative of flow velocities before shock waves in supersonic intakes, and because previous results suggested it would generate a fairly large separation bubble in the turbulent boundary layer. The exit size of the nozzle was 99 mm × 82 mm high. The experimental duct entrance was also rectangular but smaller in both dimensions so that some of the nozzle flow was spilt around the sides of the duct. This meant that none of the nozzle boundary layers entered the duct and that the heat loss from the forward portion of the duct (which could not be lagged) was minimized by having similar flow on both sides of each wall. The duct walls downstream of the nozzle exit were well insulated (see figure 1) to try to produce an adiabatic flow inside the duct. The rig was made from aluminium castings fitted with hardened steel leading edges. Continuous rubber seals were fitted between the castings as shown in figure 1.

The experimental boundary layer, on the floor of the duct, started from a leading edge in unsheared flow, had a natural transition to a turbulent layer and developed in zero pressure gradient over a distance of 0·24 m before interacting with the normal shock wave. Before the interaction the layer was approximately 3·3 mm thick and as the duct width was 85 mm, there was a layer thickness to duct width ratio of 1/26.

The height of the duct entrance was 47 mm but increased with distance downstream so that the post shock flow was subjected to an adverse pressure gradient. The roof was made of interlocking plates that were adjusted to generate a pressure gradient that was strong but did not reseparate the layer downstream of the shock wave. The sidewalls of the duct were set on slight angles to the centreline of the floor to compensate for the (calculated) growth in the sidewall boundary layer displacement thickness. Although the duct width thus increased (from 85 to 100 mm) the total layer thickness increased more rapidly and at the end of the measurement region the layer thickness to duct width ratio was approximately 1/3.

Just downstream of the shock wave, fillets were attached to all four inner corners of the duct (see figure 1) to reduce secondary flows. The thickness of the fillets increased (from zero) with

[1] And to a lesser extent by Kooi (1975), East (1976) and Abbiss *et al.* (1976).

* Actually 1·405 ± 0·01 at the exit plane, see Schofield (1975).

distance down the duct. Surface flow visualization indicated that the duct flow (away from the shock wave) was two dimensional, that there was no leakage from the duct and that the boundary layers on the other three walls did not separate.

2.2 Instrumentation

The duct floor contained forty-six small diameter static pressure tappings spaced along either side of the duct centreline (visible in figure 3*b*). In addition fifteen 20 mm diameter instrumentation holes were spaced along the centreline of the duct. Into these holes a probe traversing device could be fitted which could hold a variety of 'gooseneck' probes (single and double total head, static and total temperature). When not in use these holes were filled with aluminium plugs set flush with the test surface and sealed with 'O-ring' seals. These plugs were instrumented with either static pressure taps or copper-constantin thermocouples set in a copper bead flush with the flow surface.

The total head probes used near the wall had flattened openings measuring (typically) 1 mm × 0·12 mm with a centre of pressure estimated to be at 0·14 mm from the lower surface of the probe. The temperature probe was a standard ventilated stagnation probe with a copper-constantin thermo-couple. The opening of this probe was 5 mm × 0·38 mm with a centre of pressure estimated to be at 0·35 mm from the lower surface of the probe.

All thermocouples were referred to a standard ice point junction and the voltages generated were read with a digital voltmeter which had a resolution of 1 microvolt. The thermocouples, as well as the boundary layer and the settling chamber temperature probe, were calibrated against a standard mercury and glass thermometer in water over the range 0 to 100°C. The results for each thermocouple were fitted with a third order polynomial to be used in data reduction. As the temperatures measured in the experiments were near 120°C this procedure involved the assumption that the calibration curves could be accurately extrapolated.

The static pressure tappings were connected, using small diameter tubing, to a pressure scanning valve where the pressures were sensed with an absolute pressure transducer. Settling chamber stagnation pressure and atmospheric pressure were read in the same way. The total pressure probe was connected to one side of a differential pressure transducer while the other side was connected to the ganged wall static pressure tappings either side of the probe tip. In this way the dynamic pressure was found directly with one transducer. The pressure transducers were periodically calibrated against a deadweight tester and were always found to be linear to within 0·05% of full scale. The sensitivity for a given transducer changed less than 0·1% of full scale between calibrations. The zero pressure reading changed much more, being sensitive to changes in temperature. Consequently the zero pressure reading was taken immediately at the conclusion of each test and used in reducing that set of data.

The probe traverse incorporated a variable speed electric motor that could generate steps as small as 0·008 mm. The probe position was indicated by a linear distance transducer with a travel of 50 mm. The calibration of this transducer was found to be non-linear and affected by temperature. Consequently it was calibrated in an oven over the temperature range it attained on the rig. The two hundred calibration points were fitted using a cubic spline routine that was subsequently employed in data reduction. The temperature of the transducer on the rig was measured with a thermocouple.

A schlieren system allowed continuous viewing of the shock wave region through the windows in the duct shown in figure 1. The system also allowed spark photographs of this Schlieren pattern to be taken.

2.3 Uncertainty Estimates

The uncertainty of the experimentally measured quantities were estimated as:

$y = \pm 0{\cdot}008$ mm

$T = \pm 0{\cdot}8$ K

$p = \pm 0{\cdot}8\%$ of reading

Estimates of uncertainty for derived quantities were determined using the method of Kline & McClintock (1953) and are given below:

$u/U_1 = \pm 1{\cdot}2\%$; $\pm 2{\cdot}5\%$ near the interaction region; $\pm 4\%$ for backflow in the separation bubble.

$p_s/p_w = \pm 1{\cdot}7\%$ except near shockwaves

$T/T_{o1} = \pm 0{\cdot}3\%$

$c_f' = \pm 7\%$

2.4 Procedure

Firstly the ambient pressure was measured and used to adjust the settling chamber blowing pressure to give a correctly expanded supersonic jet at Mach 1·41 from the nozzle. The rear flap on the duct was then slowly closed until a normal shock wave appeared on the Schlieren screen. Flow conditions were then allowed to stabilize. It took approximately 30 minutes for the wall temperatures at the rear of the duct to become constant. The shock wave position was then adjusted to coincide with a marked position on the Schlieren viewing screen where it was maintained throughout the test. The wall static pressure and temperature distributions along the test surface were recorded before and after the profile data were taken. At each point in a pressure profile the probe position, probe pressure and wall pressure were recorded; in a temperature profile the recordings were: probe position, probe temperature and wall temperature.

After measurements in the main flow were complete, corresponding measurements in the shockless low speed reference layer were made. To set up this flow the settling chamber pressure was reduced so that the nozzle supplied air to the duct at Mach 0·61. This Mach number was lower than the correct post shock Mach number (0·74) behind a normal shock wave at Mach 1·41 but was the highest that could be generated without causing some supersonic flow with shock waves in the nozzle.

On the basis of results presented below, it is argued that this difference in Mach number is insignificant: it will be seen that both flows have very similar pressure gradients downstream of the normal shock position, suggesting no significant differences due to compressibility.

At the completion of these measurements the back flap was opened fully so that the flow along the duct accelerated reaching speeds up to Mach 2·3 before the end of the duct. Again wall pressures, temperatures and profile data were recorded. These supersonic results will be reported fully in a separate publication but some of the results are used in this report to check the accuracy of the temperature profile measurements.

2.5 Data Reduction

Data reduction was done with the aid of a computer program that required an input of the raw data and instrument calibration constants for each test. Profile pressures[1] were converted to Mach numbers using the isentropic flow relations. If a temperature profile had been taken for a particular station then it was interpolated with the Mach number profile to give a velocity profile. If a temperature profile was not available at that station then the simple Crocco (1932) relation,

$$T = U \tag{1}$$

was used. Comparisons (given later) with measured temperature profiles show that equation (1) gave satisfactory correlations for zero and adverse pressure gradients. In favourable pressure gradients the modified Crocco relationship

$$T = U^2 \tag{2}$$

was found to be more representative of the data.

[1] Using the probe recovery relationship given by Winter & Gaudet (1970).

The data reduction program calculated: integral boundary layer thicknesses, static temperature profiles and from these, viscosity profiles using Sutherland's equation. Density profiles were calculated by assuming the perfect gas law. The program also calculated the two dimensional stream function

$$\psi = \int_0^y \rho u dy \tag{3}$$

and a normalised enthalpy thickness

$$\epsilon = \int_0^\delta \left(\frac{\rho u T_p}{\rho_1 U_1 T_{o1}} - 1 \right) dy \tag{4}$$

Reduced data is tabulated in Table 1. Layer S denotes the main flow with the shock wave boundary layer interaction followed by the adverse pressure gradient. Layer L denotes the reference flow without a shock wave but with the adverse pressure gradient.

Skin friction coefficients were determined using Clauser's method (Clauser (1954)) which is based on writing the logarithmic law of the wall in the form,

$$\frac{u}{U_1} = \frac{u_\tau}{\kappa U_1} \log_e \frac{y U_1}{\nu} + \frac{u_\tau}{\kappa U_1} \log_e \frac{u_\tau}{U_1} + \left(\frac{u_\tau}{U_1} \right) A \tag{5}$$

and comparing data points on u/U_1, yU_1/ν axes with a family of straight lines, the slope and position of which depends on $u_\tau/U_1 (= \sqrt{c_f'/2})$. (The profiles are represented in the Appendix.) As it was calculated in the data reduction process, the local kinematic viscosity was used in calculating yU_1/ν values. Otherwise no allowance was made for compressibility. Only the two profiles upstream of the shockwave in series S would be significantly affected by compressibility. At these Mach numbers the differences in estimated skin friction between an incompressible analysis and a compressible one is of order 10%. As this variation is about the difference in values of skin friction given by different compressible methods and as the actual values for these profiles were unimportant in the analysis of this flow, only the incompressible values have been quoted.

3. RESULTS

3.1 Flow Visualization

Figure 2 shows a Schlieren spark photograph of the shock wave. It is similar to a photograph presented by Seddon (1967) for his interaction with a zero pressure gradient boundary layer. The normal shock wave bifurcates about 6 to 8 layer thicknesses above the wall, into a pair of forward and rearward facing oblique shock waves. A fine line springing from the bifurcation point indicates the existence of a vortex sheet. Such a shock structure suggests that a large separated region exists under the shock wave. The surface flow pattern (figures 3*a*, 3*b*) confirms that there is a large area of separated flow and shows that it is strongly three dimensional. Figure 3*c* presents an interpretation of the wall flow patterns. It shows the flow separating, under the shock wave, along lines (separatrices) emanating from a separation saddle point and curving slightly downstream as they approach the duct sidewalls. Directly downstream of the separation saddle is a reattachment saddle into which flow two reattachment lines. On each side of a line joining the two saddles the separated flow winds up into two counter-rotating focii.

A very similar pattern (and interpretation) is given in Green (1969) for an interaction of a turbulent boundary layer with a strong oblique shock wave in a square duct. Very similar separated regions are formed behind blocks attached to the surface in a boundary layer as shown in figure 4 (see also Castro & Robins (1977)). Hunt, Abell, Peterka & Woo (1978) made an experimental and analytical study of these separated regions. Two of their conclusions that are important to this work are: there are no closed surfaces around the separated flows and that counter-rotating vortices are shed into the downstream flow from the separated region. Supporting evidence for this last conclusion is given by Colmer (1970) who measured, at distances well downstream of a rectangular aircraft hanger, significant upflows on the centreline of flow,

suggesting the presence of streamwise vortices. Other indirect evidence is presented by Schofield & Logan (1983) who found for the two cases shown in figure 4 that the mean centreline flow recovered more quickly behind the narrower of the two blocks. The explanation offered is that for the narrow block the shed vortices are closer to the centreline and thus their mixing action is more effective on the centreline flow giving a quicker recovery.

It is theoretically possible that in the present flow vortices shed from the two focii join up and are contained within a closed separation bubble. In view of the preceding evidence it seems, however, unlikely. The existence of longitudinal vortices in the present flow offers the most plausible explanation of the results presented in this report.

The theory of flow around critical points (saddles, focii and nodes) in viscous flows has been developed considerably in the last few years (Perry & Fairlie (1974), Hunt *et al.* (1978), Perry, Chong & Lim (1982)). One aspect of the work presented in these papers is the supply of mass to vortices as they roll up and flow downstream. In the present case, mass would have to flow into the separated region to supply the vortices shed into the downstream flow. The separated region cannot therefore be closed, but must have stream tubes correcting it with the upstream flow. Thus, because open streamtubes may exist close to the wall, the separation and reattachment lines have not been joined in figure 3*c* although the oil flow pattern (which is fairly indistinct in this region) could be interpreted as supporting their junction.

3.2 Pressure Field

The wall pressure distributions measured in the two present flows are shown in figure 5 and the corresponding free stream Mach number distributions in figure 6. Although the Mach number after the shock wave in layer S was higher than the nozzle Mach number in layer L, differences in turbulence structure due to compressibility would have been very small. Importantly, pressure gradients of the two flows appear very similar (see figures 7 and 8). Since pressure gradient is the dominating factor in boundary layer development it is argued that layer L is a good reference layer.

In both separating flows investigated by Simpson *et al.* (1977 and 1981) separation occurred just before the pressure gradient dropped to a near zero constant value. In the present results separation occurs before a constant value of pressure gradient is attained. Perry & Fairlie (1974) have presented analysis and experimental results which suggest that separation and reattachment points coincide with the pressure gradient becoming (locally) zero. As shown in figure 8 the present results do not support this proposal.

The shape of the initial wall pressure rise under the shock wave appears to be governed mainly by the shock strength. Figure 9 shows that the wall pressure rise in the early stages of the interaction in the present flow is similar to that in Seddon's flow which did not have a post-shock pressure gradient. To compare the results the downstream distance has been non-dimensionalized with the undisturbed boundary layer displacement thickness. It is seen later that in the present flow, the post-shock adverse pressure gradient produces large changes to the flow structure but apparently it has little effect on the shape of the initial pressure rise. This is consistent with the concept of a 'free interaction' proposed by Chapman, Kuehn & Larsen (1957) in which, provided a shock wave induced separation, the flow upstream of the separation point was not much affected by downstream conditions.

The Prandtl boundary layer approximation leads to $\partial p_s/\partial y \simeq 0$ which is a very good approximation for layer L (the flow without a shock wave) as shown in figure 10. Near a shock wave however, it is certain that $\partial p_s/\partial y$ cannot be zero as the streamwise pressure distribution changes from the wall distribution shown in figure 5 to a step distribution in the flow above the shock bifurcation point. The surface flow pattern of figure 3 suggests that the static pressure will also vary laterally across the flow. The static pressure field near the separation bubble varies, therefore, in all three directions.

In the present work the static pressure was assumed to be constant through the boundary layer. A few static pressure profiles were recorded (figure 11) and they show this to be an acceptable approximation for flow near reattachment and downstream from it. Upstream of reattachment, near separation and the shock waves, is a most difficult area to obtain accurate static pressure measurements in the flow and it was not attempted here. However the magnitude or even the sign of departure from the constant pressure assumption is far from clear. Seddon's limited

measurements in this region show no static pressure variation within the boundary layer but significant variation outside it up to the height of the bifurcation. Kooi (1975) measured four static profiles near the shock wave but all were quite different from Seddon's result as they showed significant variation within the boundary layer. To further confuse the issue Kooi's profiles were radically different in shape between themselves, even those spaced only $0{\cdot}8\delta$ apart. This conflicting data suggests that the assumption of constant static pressure is as good as any at present. This uncertainty is reflected in the larger uncertainty estimate for u/U_1 measurements in the interaction region (Section 2.3).

3.3 Velocity Field

Velocity profiles were measured only on the centreline of the flow. In the interaction region profiles off the centreline will vary significantly. Downstream of the interaction, the surface flow tests suggest that the centreline should be representative of the flow over most of the width. The velocity and density[1] profiles have been used to generate the function

$$\psi = \int_0^y \rho u dy.$$

For two dimensional flow ψ is the stream function. Areas of the interaction flow are, however highly three dimensional and in these regions ψ will not give streamlines. However the present mean velocity measurements were taken on the duct centreline and here flow symmetry would require three dimensionality or crossflows to be negligible. On the centreline then ψ will probably approximate the stream function. Figure 12 shows the centreline streamlines with the (Mach) profiles used to calculate them. An average shock system taken from the spark schlieren photographs is also shown.

The data in this diagram is internally consistent, the streamline flow angles show good agreement with the flow deflections of the shock system and the values of ψ given by different profiles form a consistent streamline pattern.[2] However there are four factors that could affect the accuracy of this diagram:

(i) static pressure variations through the boundary layer,

(ii) As figure 3*b* shows, the line of symmetry of the separated flow does not quite coincide with the duct centreline and thus crossflows on the duct centreline may not be negligible.

(iii) velocity vectors have been assumed to be normal to the pitot probe opening whereas Abbiss *et al.* (1976) showed that near the shock wave, flow angles could be as large as 8° to the x axis,

(iv) the reversed profiles were measured with (small) pitot probes and Simpson (1976) claims that they cannot accurately measure backflow with its intermittent flow reversals and consequent large changes in velocity magnitude and direction.

The effects of (ii) and (iii) can be estimated and are small. The magnitude of (i) cannot be confidently assessed but is unlikely to be significant over the entire flow map. Finally the magnitudes of the reversed flow inferred from the pitot tubes was similar to those found by Simpson *et al.* (1977, 1981) using laser anemometry. Figure 12 therefore, is probably a fairly accurate drawing of the centreline streamline pattern.

---

[1] Density was calculated by the data reduction program from the perfect gas law, using either the calculated or measured static temperature profile and assuming constant static pressure.

[2] The separation point has been shown connected to the reattachment point although it is quite possible that an 'alleyway' exists in the vertical plane to supply mass into the separated region. However, the streamline plots in the figure are not accurate enough to determine such detail (see main text).

Figure 13 compares a non-dimensionalized version of this streamline pattern with the one by Seddon for a flow with no post shock pressure gradient. There are substantial differences between them which can be explained by the effect the post shock adverse pressure gradient has in delaying reattachment and hence creating a larger separation region than in Seddon's flow. In the present flow the rapid increase in displacement thickness caused by the larger separated region requires larger streamline deflections. Consequently the shock wave system is tipped forwards and upwards away from the wall compared with the pattern measured by Seddon. Mach number profiles suggest that a large supersonic tongue is formed behind the shock wave. Seddon's measurements also suggested a supersonic tongue but his flow had a higher incident Mach number (1·47). Flows at the same Mach number (1·4) without a post shock pressure gradient (East (1976), Kooi (1975)) did not apparently contain supersonic tongues. Apparent inconsistencies between these results are impossible to resolve with the current evidence. All results involve some uncertainty in the Mach number profiles near the shock wave, mainly due to inaccuracies in measuring the static pressure. Within the supersonic tongues the Mach numbers exceed unity by small amounts and small differences in static pressure are sufficient for a supersonic tongue to appear or disappear in the results.

3.3.1 Displacement Thickness

The distribution of displacement thickness in the interaction region is compared with those for flows without post shock pressure gradients in figure 14. The three comparison flows have similar Mach and Reynolds numbers but have much smaller growths in displacement thickness through the interaction than the present layer. After reattachment the displacement thickness of the layers without a post shock pressure gradient continues to decrease. This is because the layer is relaxing back to zero pressure gradient flow conditions and velocities near the wall increase rapidly, causing the displacement thickness to decrease. In the present flow however, the layer after reattachment continues to be subjected to a severe adverse pressure gradient which causes high rates of mass entrainment into the layer. Although flow acceleration near the wall again would tend to decrease the displacement thickness, the entrainment rate of the layer is so large that in this case the displacement thickness increases quite rapidly after reattachment.

Figure 15 compares the early displacement thickness growth for the present layers S and L. The comparison shows that in the region where the pressure gradients for the two layers are similar (i.e. after the reattachment position) the displacement thickness growth rates for them are very similar. The growth rates are high while the local pressure gradient is high but when the pressure gradients drop (see figure 8) the layers go through identical relaxations where the velocity near the wall increases and the displacement thickness therefore decreases. At the completion of this process the displacement thicknesses begin to increase again by entrainment. The rates are closely similar, which might be expected as the two layers are developing in similar pressure gradients. This figure would suggest therefore that the effect of the shock wave on displacement thickness is limited to a simple constant addition to the thickness. It might appear therefore that the effects of shock wave and pressure gradient are independent, with the shock wave having only a local effect on the layer (shown in figure 15) and the pressure gradient determining boundary layer development downstream of the shock wave. However this is not the case. Figure 16 plots the displacement thickness growth for the two layers through the whole downstream mixing region. To give a fair comparison of growth rates in this mixing region, the displacement thickness has been non-dimensionalized with its value at the start of the region ($x = 0{\cdot}403$ m); in this way the difference in displacement thickness due to the shock wave in layer S is removed from the downstream comparison. The figure shows that the displacement thickness grows much faster for the layer without the shock wave and would probably separate before the layer which has interacted with a shock wave.

The explanation proposed here for this difference between the two layers is that vortices are shed from the separated region under the shock wave and have an important effect on flow downstream of the high pressure gradient region by increasing mixing in the layer, stabilizing it and slowing its growth. This conclusion is supported by analysis of other boundary layer parameters in the following sections.

3.3.2 Boundary Layer Shape Factors

In figure 17, the standard boundary layer shape factor (δ^*/θ) is compared with Seddon's results for no post shock pressure gradient. The main difference between the results is in the separation region and is due to the enlargement and extension of the separated flow by the adverse pressure gradient in layer *S*. After reattachment the results are similar in this interaction region.

Figure 18 compares the shape factor variation with that of the shockless reference layer through the downstream mixing region. These results again indicate that the shockless layer will separate first as it has a larger value of *H* throughout the mixing region and is increasing quite rapidly at the last observation.

Similar conclusions can be drawn from the variations of two other shape factors: Clauser's shape factor,[1] (*G*, figure 19) and Cole's wake strength parameter[2] (Π, figure 20).

3.3.3 Skin Friction

Comparisons of skin friction coefficient for the two present layers (figure 21) show that downstream of the interaction the shockless layer is moving towards separation while the results of the layer with a shockwave are nearly constant with distance.

In the interaction region where shockwave forces dominate, comparisons with flows that do not have post shock pressure gradients are interesting. Some results given by Seddon (figure 22) show that the skin friction coefficient has overshot the undisturbed value while other results by Kooi (1975) suggest that they may also overshoot the undisturbed value further downstream. Figure 22 shows that the present results don't do this. A simple explanation for this difference is that in all the flows longitudinal vortices are generated at the interaction and have a strong stabilizing effect on the downstream flow. In the absence of other forces these vortices quickly increase the skin friction coefficient of the flows above their upstream undisturbed values. In the present flow however the effect of the vortices are counteracted in part by the destabilizing effect of the post shock adverse pressure gradient. This interaction results in the skin friction stabilizing at a lower value than the upstream undisturbed value.

It seems from figure 21 that the vortex mixing persists for a long distance downstream. This long persistence of the mixing vortices is important in considering the question raised by Seddon: what length of flow development is required for the layer to return to its undisturbed state? The above discussion implies that for layers with or without post shock pressure gradients, the mixing vortices initiated at the separation bubble would have to decay before the relaxation process can commence. The present results show no indication of such a decay at the last observation (which corresponds to an x/δ^* value of 4000) and it seems likely therefore that a return to an 'undisturbed state' will require a distance so large that it would be of little practical interest.

3.4 Temperature Field

3.4.1 Wall Temperatures

The centreline wall temperature variation for the shock wave layer (*S*) is compared with the theoretical adiabatic wall temperature distribution[3] for zero pressure gradient flows in figure 23. As the measured temperature distribution is lower in value than the adiabatic distribution there is a net heat flow from the plate to its lower temperature surroundings. Near the reattachment point the wall temperature approaches the stagnation temperature but this is followed downstream by a local minimum in wall temperature which coincides with the region of large accelerations in the flow near the wall. Downstream of this region the wall temperature is maintained at a little less than the (zero pressure gradient) adiabatic distribution.

---

[1] Clauser (1954).

[2] Coles (1956).

[3] Using a wall recovery factor of $Pr^{1/3}$.

Figure 24 shows the normalized enthalpy thickness as a proportion of total layer thickness along the flow. The normalized enthalpy thickness of a boundary layer is that thickness of flow at free stream conditions that would account for the difference between local and free stream enthalpy integrated across the boundary layer. It is a (total) heat energy displacement thickness and is positive for heat flowing into the layer and negative for heat flowing out of the layer. Figure 23 shows that it is mainly negative along this flow but in all cases is small amounting to less than 0·5% of the total heat in the boundary layer.

The heat loss from the plate in layer L is greater as indicated by the wall temperature distribution[1] shown in figure 25. In this case the temperature distribution varies slowly and continuously with distance and is much further below the zero pressure gradient wall adiabatic temperature distribution. This is to be expected as the temperature of the air supplied to the experimental duct was the same for both layer L and S but the mass flow and hence heat supplied for layer L was only 38% of that supplied for layer S. The duct heat loss[2] for layer L was thus a higher proportion of the heat supplied to the duct and resulted in the larger temperature drops shown in figure 25.

3.4.2 Temperature Profiles

The temperature profiles measured here in strong adverse pressure gradients are unusual, particularly those through or near the separated region. As the temperature differences between the flow and the wall were small and the probe was a simple shielded thermocouple it was thought desirable to check the reliability of the instrumentation and measuring techniques. This was done by measuring temperature profiles in a shockfree adiabatic favourable pressure gradient flow and comparing them with reliable data that exists for these flow conditions. The flow was generated by opening the rear flap of the duct to give an accelerating supersonic flow with Mach numbers up to 2·3. The wall temperature results, figure 26, shows that the centreline distribution was close to (... pressure gradient) adiabatic conditions. The temperature profiles (figure 27) may be compared with those of Meier & Rotta (1..., ... measurements in a supersonic nozzle using a most sophisticated probe that drew air through a range of choked orifices. Both the present flow and that of Meier & Rotta were closely adiabatic and had mild favourable pressure gradients. The data are thus directly comparable.

Both sets of temperature profiles (the present ones and those of Meier & Rotta) have a sinuous shape that crosses the Crocco line ($\bar{T} = \bar{U}$) before overshooting the free stream stagnation temperature ($\bar{T} = 1$). The size of the temperature overshoots were slightly different in the two layers. For adiabatic flow, conservation of energy requires that the average stagnation enthalpy across the layer should equal the free stream enthalpy. This is obviously not fulfilled in the present profiles as the temperature overshoots are too small to compensate for the temperature deficits near the wall. However they are consistent with ... heat flow out of the layer. As the Meier & Rotta flow was closer to adiabatic conditions than the pres... their profiles had larger overshoots. Overall then the consistency of these results gave some confidence in the present temperature measurements.

The temperature profiles in the shock free adverse pressure gradient flow (layer L) are quite different from the favourable pressure gradient results. Figure 28 shows that while these profiles still have a sinuous shape they do not cross the Crocco line ($\bar{T} = \bar{U}$) but lie between it and the free stream stagnation line. None of the profiles show an overshoot which is consistent with a ...tively large heat flow out of this layer.

As might be expected, the temperature profiles for the shockwave layer (S) differ from the previous results only in the vicinity of the interaction. Figure 2... shows that downstream of the interaction region ($x > 0{\cdot}4$ m), the profiles are similar to those in layer L differing only ... they have overshoots in total temperature as expected for near adiabatic conditions.

[1] And the values of ϵ/δ, see table 1.

[2] As the density is lower in layer L, the heat transfer coefficient from the flow to the duct wall will be lower and thus the overall heat transfer from the duct will be slightly less. This however will be a small effect compared with the large difference in duct mass flow.

The profiles around the separated region are quite unusual. As yet there is no theory that can suggest what mechanisms in the boundary layer cause such distributions in total temperature. The best that can be done is to try and correlate the flow behaviour at each station with the total temperature distributions. The profile at $x = 0{\cdot}249$ m passes through the recirculating fluid[1] and displays a nearly constant total temperature across the layer. The outer part of the profile suggests that the upstream wall fluid lifted over the backflow has been fully mixed. This is supported by the results of Simpson *et al.* (1981) who made Reynolds stress measurements after detachment which implied very high rates of mixing just outside the reversed flow region. The profile at $x = 0{\cdot}276$ m has a large overshoot and is nearly adiabatic (see figure 24). It was positioned very close to the reattachment saddle where the flow is strongly decelerating and is similar to a stagnation flow with a wall temperature that approaches the adiabatic value. In contrast the profile at $x = 0{\cdot}314$ m has a low average total temperature. It was positioned in a region where the wall flow was undergoing rapid acceleration.

4. DISCUSSION AND CONCLUSION

The major conclusion of this experiment is that the effects of the normal shock wave and the adverse pressure gradient did not combine to produce a boundary layer near separation but rather that the interaction acted as a stabilizing agency for the boundary layer in the adverse pressure gradient. This result will be relevant to flows in most rectangular supersonic air intakes and diffusers. Its relevance to axisymmetric air intakes, transonic aerofoils and transonic compressor stages is more doubtful. While it is theoretically possible that these flows are two dimensional with closed separation bubbles, in practice however the flows will be three dimensional to varying degrees and may even develop cellular flow patterns shedding vorticity downstream. Although the level of this vorticity is likely to be considerably less than that in the present experiment, it may have a significant effect on the downstream layer. However, there is another possible source of vorticity which could be important in these nominally two dimensional flows. It is likely that Taylor–Goertler vortices would be generated in the flow over the rear of the separation bubble as a consequence of the change in angular velocity in this region. These speculations are somewhat supported by the work of Livesey & Odukwe (1974), Odukwe & Livesey (1974) and Kamal & Livesey (1977). These workers have measured the performance of a range of subsonic axisymmetric diffusers preceded by a long inlet pipe. They found that the diffusers gave higher overall pressure recovery and lower outlet distortion (two factors closely related to boundary layer separation) if the inlet pipe flows contained normal shock waves. The origin of this stabilization was attributed to the (measured) increased turbulence level. The differences in diffuser performance were large, suggesting an intense distributed mixing agency such as longitudinal vortices.

The present results are probably not relevant to the case where the shock wave is too weak to separate the boundary layer. Here the adverse effects of shock wave and pressure gradient on boundary layer development may be additive in some way. Paradoxically, component performance will be enhanced in some cases by the presence of strong normal shock wave with its local separation, as this has the same effect as a pair of vortex generators at the start of the subsonic pressure rise.

Another conclusion of this work is that the post shock pressure gradient, as well as having a large effect on the downstream boundary layer development, has a gross effect on the structure of the interaction region itself. Compared with the zero pressure gradient case, the adverse pressure gradient delays boundary layer reattachment which greatly increases the size of the separated region. This causes the shock waves to move forward and upwards away from the wall. The resulting shock system is differently shaped compared with the zero pressure gradients case. It follows therefore that results for normal shock wave–boundary layer interactions without a post shock pressure gradient are poor guides to interactions in most practical flows which involve post shock pressure gradients.

[1] Values of T_P are unreliable here as measurements with the temperature probe facing downstream into the reversed flow were not attempted.

A plausible explanation of boundary layer behaviour in flows with normal shock waves can be made in terms of: the shock wave, the post shock adverse pressure gradient and vortices shed from the interaction region. The shock wave dominates flow development in its immediate region but although its effects (separation and a rapid rise in displacement thickness) are drastic, they are also shortlived. Similarly an adverse pressure gradient tends to increase the displacement thickness and decrease the skin friction of the layer but these effects can be significantly modified by mixing caused by longitudinal vortices. For flows with a shock wave the longitudinal vortices quickly restabilize the boundary layer after reattachment, causing the skin friction to overshoot its undisturbed value. For flows with a shock wave and a subsequent adverse pressure gradient, longitudinal vortices continue to move the layer away from the condition of a corresponding shock free reference layer. The vortices appear to be very long lived, as this process continues to distances large compared with distances of practical interest.

The temperature results show that the shape of the mean temperature–velocity profiles depend on the sign of the pressure gradient and the local heat transfer rate. Profiles can be quickly and markedly distorted by unusual local flow conditions such as a nearby separation or reattachment point or by backflow within a separation region. In adverse pressure gradient flow, the temperature velocity profiles lie between the Crocco formula and the free stream stagnation temperature. In favourable pressure gradient flow they lie between the Crocco and the modified Crocco formulae.

REFERENCES

Abbiss, J. B., East, L. F., Nash, C. R., Parker, P., Pike, E. R. and Sawyer, W. G. (1976). RAE TR 75141.

Alber, I. E., Bacon, J. W., Masson, B. S. and Collins, D. J. (1973). A.I.A.A. Jnl, Vol. 11, No. 5, pp 620–627.

Alstatt, M. C. (1977). A.E.D.C. Rept. AEDC-TR-77-47.

Brown, A. C., Nawrocki, H. F. and Paley, P. N. (1968). Subsonic Diffusers Designed Integrally with Vortex Generators. J. of Aircraft, Vol. 5, No. 3, pp 221–229.

Coles, D. E. (1956). J. Fluid Mech., Vol. 1, p. 191.

Coles, D. E. and Hirst, E. A. (1968). AFOSR-IFP Stanford Conference on Turbulent Boundary Layer Prediction Vol. II, Stanford University.

Clauser, F. H. (1954). Jnl Aero. Sci., Vol. 21, pp 91–108.

Clauser, F. H. (1956). Adv. in Appl. Mech., Vol. 4, p. 21.

Colmer, M. J. (1970). R.A.E. TR 70202.

Crocco, L. (1931). Rendiconti R. Accadami dei Lincei. Vol. 14, p. 490.

East, L. F. (1976). RAE Tech. Memo. Aero. 1666.

East, L. F., Sawyer, W. G. and Nash, C. R. (1979). RAE Tech. Rept. No. 79040.

Green, J. E. (1969). RAE TR 69098.

Hunt, J. C. R., Abell, C. J., Peterka, J. A. and Woo, H. (1978), J. Fluid Mech., Vol. 86, pp 179–200.

Inger, G. R. (1975). Final Report to Office of Naval Research. Contract No. N0014-75-C-0456.

Inger, G. R. and Mason, W. H. (1975). Virginia Polytechnic Institute and State University, Rept. VPI-Aero-029.

Kamal, W. A. and Livesey, J. L. (1977). Proc. of Symposium on Turbulent Shear Flows, University Park, Pennsylvannia.

Kamal, W. A., Odukwe, A. O. and Livesey, J. L. (1974). Proc. of 5th Australasian Conf. on Hydraulics and Fluid Mech., New Zealand.

Kline, S. J. and McClintoch, F. A. (1953). Mech. Eng'g. Vol. 75, pp 3–8.

Kooi, J. W. (1975). AGARD Symposium on Flow Separation, AGARD-CPP-168.

Little, B. H. (1967). V.K.I. TN 39.

Livesey, J. L. and Odukwe, A. O. (1974). Proc. Instit. of Mech. Engs. Vol. 188, 56/74, p. 607.

Mateer, G. G., Brosh, A. and Viegas, J. R. (1976). A.I.A.A. paper 76-161.

Meier, H. U. and Rotta, J. C. (1971). A.I.A.A. Jnl, Vol. 9, No. 11, p. 2149.

Padova, C., Falk, T. J. and Wittliff, C. E. (1980). A.I.A.A.-paper-80-0158.

Perry, A. E. and Fairlie, B. D. (1974). Adv. Geophys., B18, p. 299.

Perry, A. E. and Fairlie, B. D. (1975). J. Fluid Mech., Vol. 69, p. 657.

Perry, A. E. and Lim, T. T. (1978). J. Fluid Mech., Vol. 88, p. 451.

Schofield, W. H., Lin, S. and Logan E. (1983). Proc. 6th Australasian Conf. on Hydraulics and Fluid Mech., Newcastle.

Seddon, J. and Haverty, L. (1954). RAE Tech. Note Aero. 2329.

Seddon, J. (1967). ARC R & M No. 3502.

Simpson, R. L. (1976). A.I.A.A. Jnl, Vol. 14, p. 124.

Simpson, R. L., Strickland, J. H. and Barr, P. W. (1977). J. Fluid. Mech, Vol. 79, pp 553–594.

Simpson, R. L., Chew, Y. T. and Shivaprasad, B. G. (1981). J. Fluid Mech., Vol. 113, pp. 23–51.

Stewart, D. G. and Fisher, S. A. (1970). Aust. Dept. of Supply, Aero Res. Labs. Report ME 129.

Vidal, R. J., Wittliff, C. E., Catlin, P. A. and Sheen, B. H. (1973). Proc. A.I.A.A. Fluid & Plasma Dynamics Conf., Palm Springs Calif. pp 1–14.

Vidal, R. J. and Kooi, J. W. (1976). NLR Rept. AC-76-02.

Vidal, R. J. and Catlin, P. A. (1977). Calspan Rept. WF-5746-A-1.

Winter, K. G. and Gaudet, L. (1970). ARC 3712.

TABLE 1

Summary of Results

x (m)	δ (mm)		δ^* (mm)		θ (mm)		H	
Layer:	S	L	S	L	S	L	S	L
0·156	2·4	2·6	0·317	0·407	0·247	0·298	1·284	1·367
0·199		4·5		0·743		0·528		1·407
0·212	3·3	4·7	0·330	0·935	0·263	0·634	1·254	1·476
0·225	3·6	5·2	0·840	1·039	0·534	0·681	1·574	1·526
0·237	6·5	6·0	2·417	1·688	0·645	0·993	3·745	1·700
0·249	8·9	6·7	4·062	1·504	0·460	0·926	8·838	1·624
0·263	8·8	6·8	4·180	1·705	0·408	1·031	10·235	1·654
0·276	8·5	8·1	2·948	2·062	0·493	1·133	5·979	1·821
0·288	9·4	8·1	3·132	1·919	1·338	1·178	2·341	1·628
0·314	11·1	10·0	3·143	2·031	1·560	1·300	2·014	1·562
0·340	15·3	10·5	4·057	2·677	2·238	1·653	1·812	1·619
0·375	19·0	15·6	4·122	3·481	2·527	2·246	1·631	1·550
0·403	13·4	10·8	2·396	1·774	1·712	1·265	1·400	1·402
0·434	13·4	13·0	2·453	2·110	1·680	1·502	1·460	1·405
0·586	25·7	21·5	5·016	4·250	3·623	3·005	1·384	1·414
0·737	30·0	27·4	5·000	6·469	3·520	4·058	1·420	1·594
0·890	36·1	36·6	6·413	8·648	4·652	5·427	1·379	1·593
1·042	29·6	38·0	5·003	9·473	3·720	6·264	1·345	1·512
1·194	43·3	39·0	8·758	12·50	5·958	7·243	1·470	1·726
1·347	48·2	52·0	6·868	13·09	4·743	6·918	1·448	1·893
1·499	35·3	42·2	5·856	12·83	4·413	7·996	1·327	1·630
x (m)	M_1		ρ_1 (kg/m^3)		ϵ/δ		C_P	
Layer:	S	L	S	L	S	L	S	L
0·156	1·388	0·608	1·259	0·986			−0·016	−0·017
0·199		0·547		0·993			+0·003	+0·003
0·212	1·395	0·526	1·238	1·014			+0·003	+0·076
0·225	1·405	0·506	1·289	1·025	−0·00104	−0·00292	+0·248	+0·150
0·237	1·102	0·479	1·689	1·055			0·390	0·220
0·249	1·031	0·462	1·744	1·077	+0·00055	−0·00266	0·455	0·276
0·263	0·986	0·461	1·845	1·063			0·502	0·312
0·276	0·918	0·424	1·898	1·050	+0·00158	−0·00130	0·567	0·337
0·288	0·909	0·454	1·929	1·038			0·614	0·356
0·314	0·859	0·436	2·036	1·056	−0·00408	−0·00370	0·689	0·387
0·340	0·821	0·426	2·075	1·065			0·744	0·412
0·375	0·774	0·423	2·069	1·063			0·784	0·429
0·403	0·763	0·416	2·114	1·080	+0·00075	−0·00286	0·823	0·445
0·434	0·711	0·406	2·145	1·088	−0·00289	−0·00316	0·852	0·453
0·586	0·636	0·371	2·242	1·093			0·959	0·526
0·737	0·562	0·345	2·317	1·098	−0·00243	−0·00281	1·055	0·604
0·890	0·492	0·318	2·361	1·121	+0·00051	−0·00167	1·109	0·647
1·042	0·420	0·274	2·447	1·129	−0·00347		1·154	0·692
1·194	0·385	0·248	2·443	1·115	−0·00296	−0·00425	1·191	0·730
1·347	0·336	0·247	2·483	1·152			1·205	0·749
1·499	0·306	0·244	2·375	1·126			1·208	0·749

TABLE 1 (Continued)

Summary of Results

x (m)	G		Π		dC_p/dx (m^{-1})	
Layer:	S	L	S	L	S	L
0·156	6·41	7·71	0·76	1·39	0·41	1·12
0·199		8·57		1·24	0·61	5·41
0·212	5·66	10·25	0·32	1·70	15·0	5·61
0·225	18·04	11·51	4·76	2·02	12·0	6·05
0·237		17·14		3·94	7·50	4·89
0·249		15·21		3·14	5·30	3·68
0·263		16·23		3·51	4·20	3·37
0·276		20·50		4·04	3·50	2·53
0·288	50·66	14·45	12·40	2·70	3·10	1·58
0·314	36·01	12·75	8·69	2·16	2·34	0·59
0·340	23·89	14·26	5·04	2·56	1·45	0·22
0·375	18·14	13·22	3·60	2·40	0·90	0·43
0·403	10·48	9·14	1·63	1·29	0·69	0·49
0·434	12·30	8·95	2·13	1·08	0·54	0·67
0·586	10·47	10·01	1·58	1·74	0·68	0·69
0·737	10·85	14·19	1·31	2·36	0·42	0·56
0·890	10·37	15·20	1·54	2·80	0·33	0·40
1·042	9·13	13·08	3·18	2·50	0·27	0·30
1·194	12·64	19·81	2·72	4·40	0·18	0·21
1·347	11·49	21·08	1·59	3·58	0·06	0·04
1·499	8·33	15·47	0·95	2·70	−0·04	−0·05

x (m)	c_f'		δ_e (mm)	
Layer:	S	L	S	L
0·156	0·00239	0·00232	2·10	1·90
0·199		0·00228	3·10	4·00
0·212	0·00267	0·00197	2·40	4·20
0·225	0·00084	0·00180		4·40
0·237	Neg.	0·00109		4·80
0·249	Neg.	0·00128		5·50
0·263	Neg.	0·00125		6·40
0·276	Neg.	0·00096		7·00
0·288	0·00026	0·00142	9·20	7·90
0·314	0·00040	0·00160	9·80	9·20
0·340	0·00071	0·00143	14·60	11·40
0·375	0·00092	0·00143	16·00	14·10
0·403	0·00150	0·00202	13·50	9·10
0·434	0·00133	0·00208	12·00	11·70
0·586	0·00141	0·00170	30·40	23·20
0·737	0·00150	0·00135	28·00	28·00
0·890	0·00141	0·00119	39·20	36·00
1·042	0·00158	0·00133	32·40	46·40
1·194	0·00126	0·00090	48·40	49·40
1·347	0·00145	0·00100	49·20	66·00
1·499	0·00175	0·00120	35·40	42·00

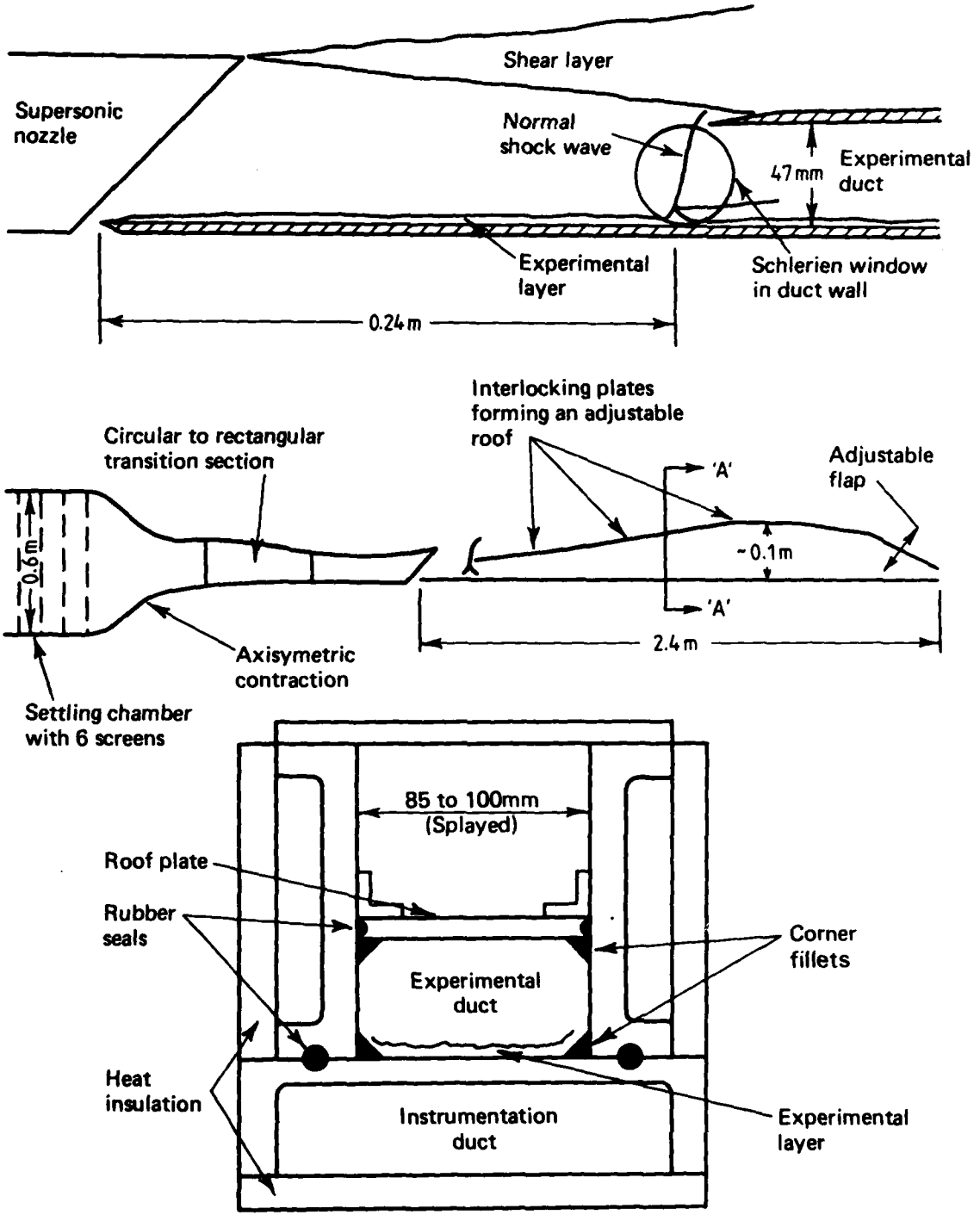

FIG. 1 EXPERIMENTAL RIG

FIG. 2 SCHLIEREN SPARK PHOTOGRAPH OF NORMAL BIFURCATED SHOCK WAVE. The wall is approximately 1/10th of the window diameter below the bottom of the window.

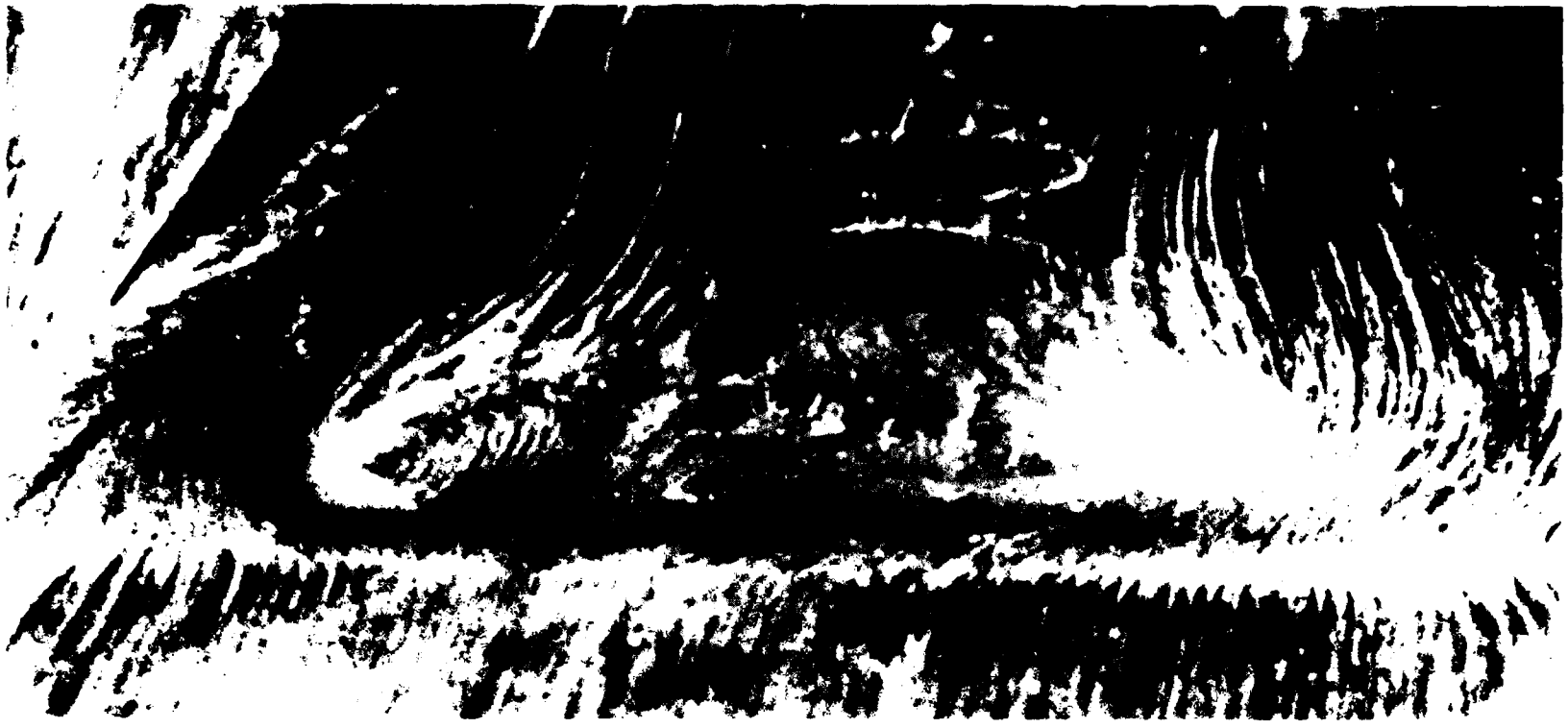

FIG. 3 SURFACE OIL FLOW PATTERN

(a) Downstream view of interaction region

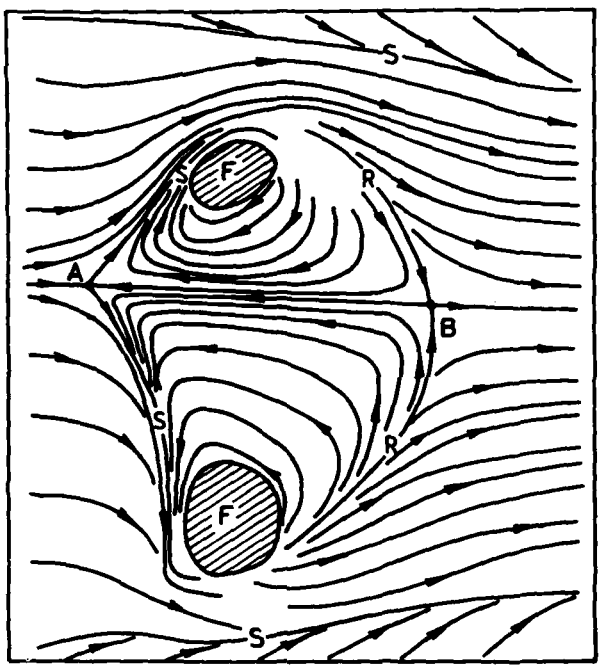

FIG. 3 (Continued)

(b) Plan view of surface flow in the interaction region

(c) Schematic interpretation of Fig. 3(b)
A – Separation saddle point
B – Reattachment saddle point
F – Focus
S – Separation line

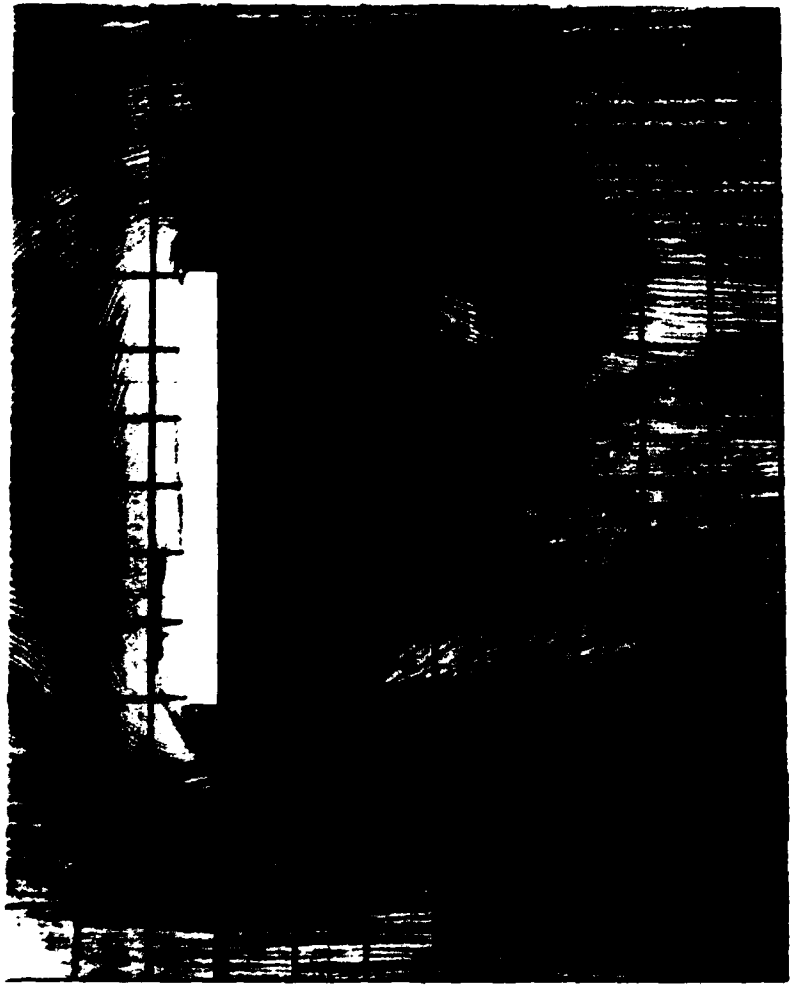

(a) Square prism (length/width = 9)

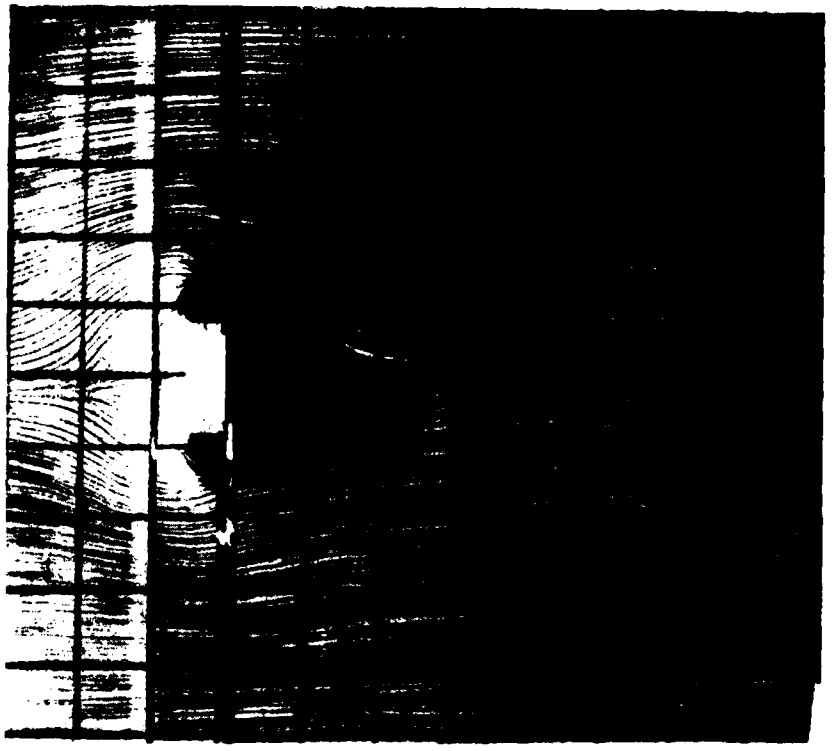

(b) Square prism (length/width = 3)

FIG. 4 SEPARATED REGIONS BEHIND PRISMS ATTACHED TO THE WALL IN A TURBULENT BOUNDARY LAYER
(Schofield & Logan (1983))

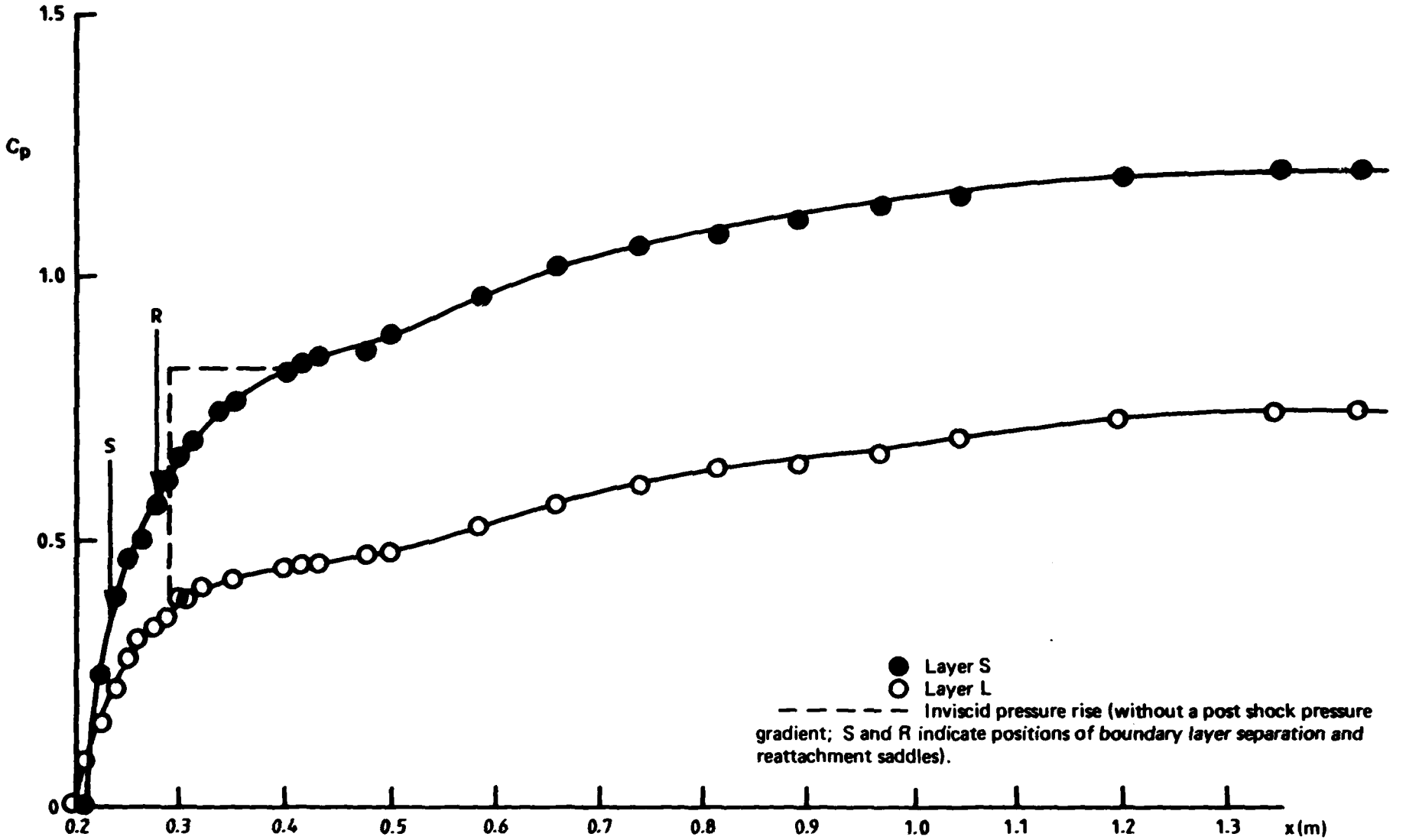

FIG. 5 WALL PRESSURE DISTRIBUTIONS

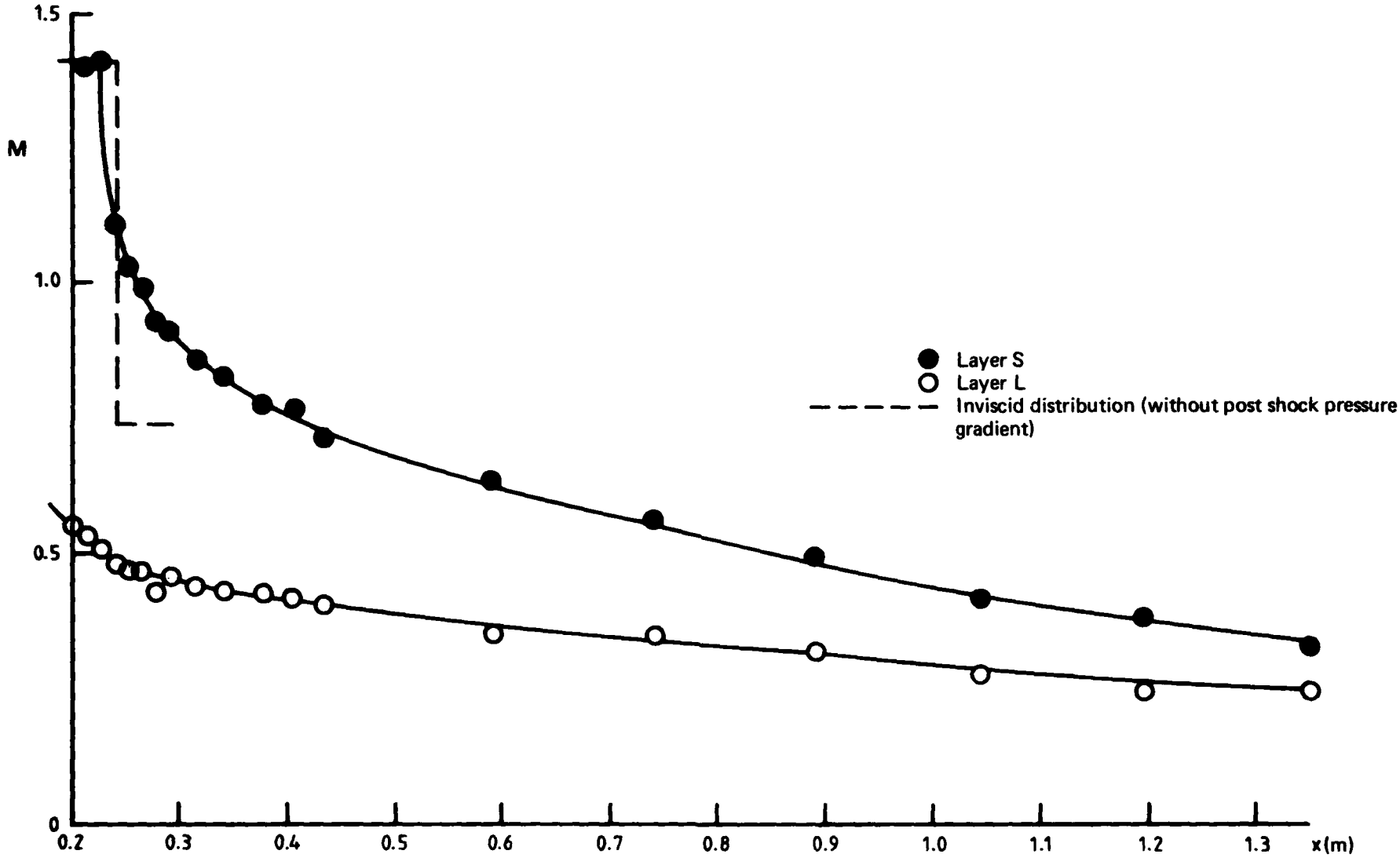

FIG. 6 MACH NUMBER DISTRIBUTIONS

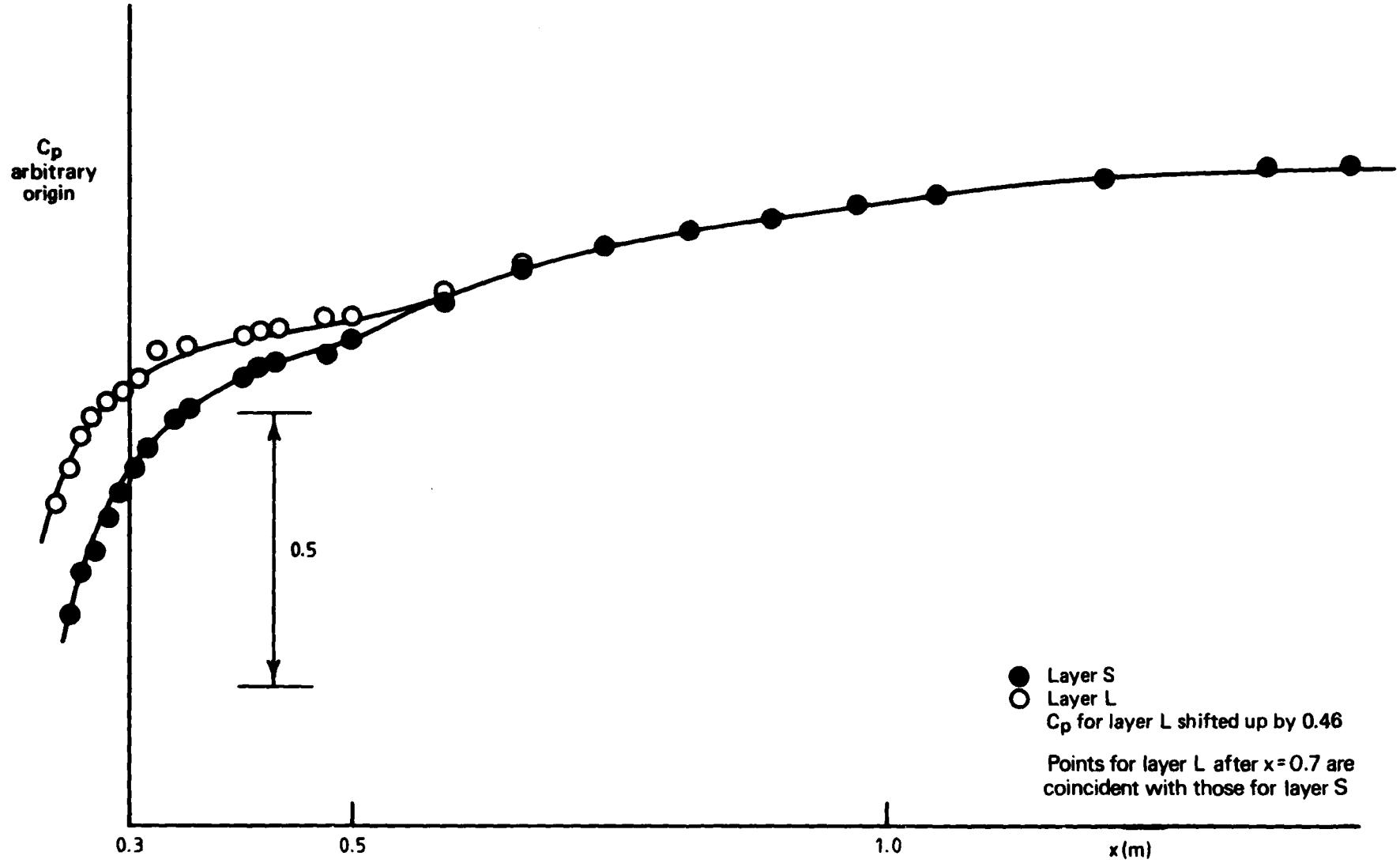

FIG. 7 WALL PRESSURE DISTRIBUTIONS SHIFTED TO SHOW SIMILARITY.

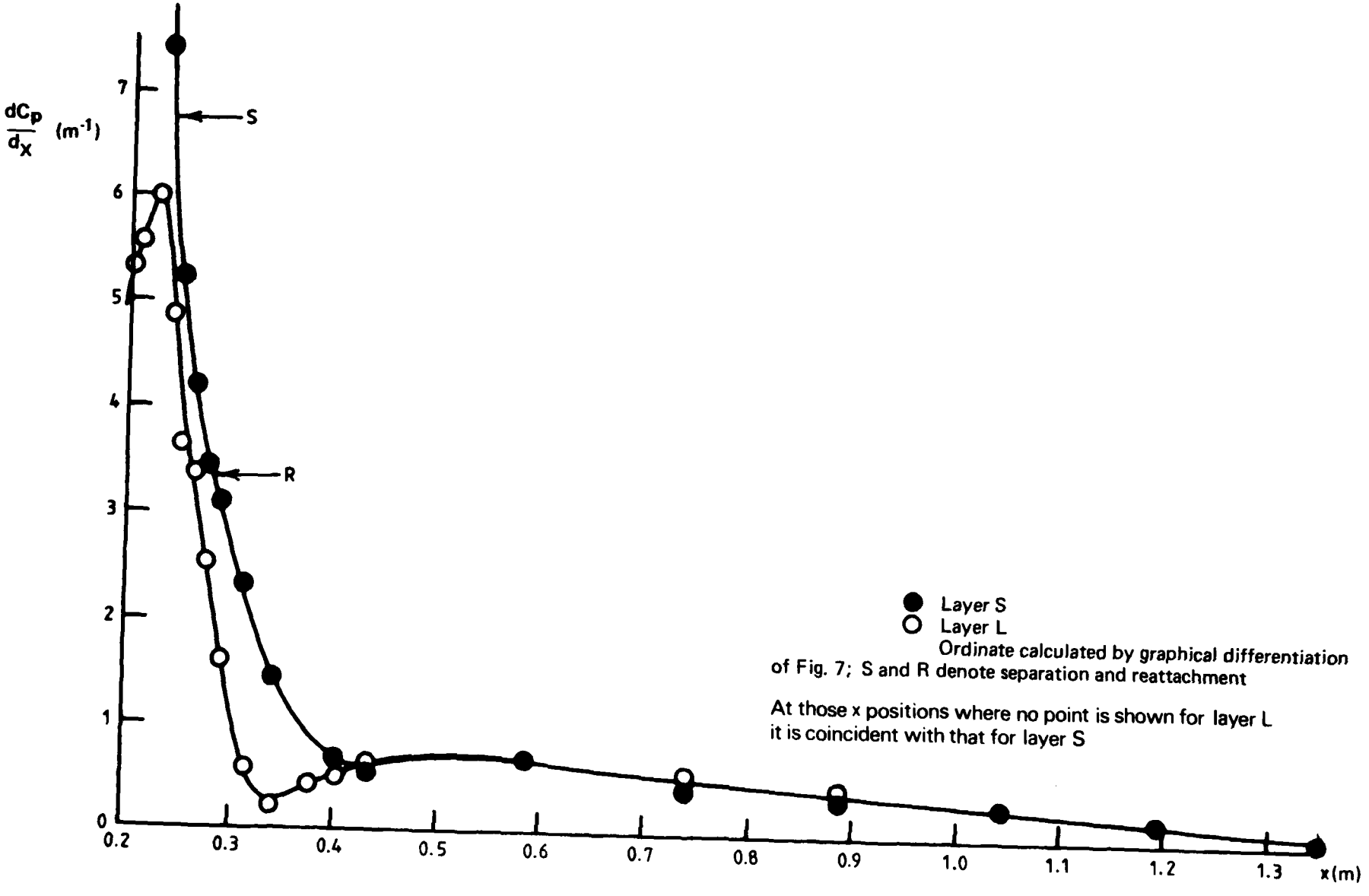

FIG. 8 PRESSURE GRADIENTS.

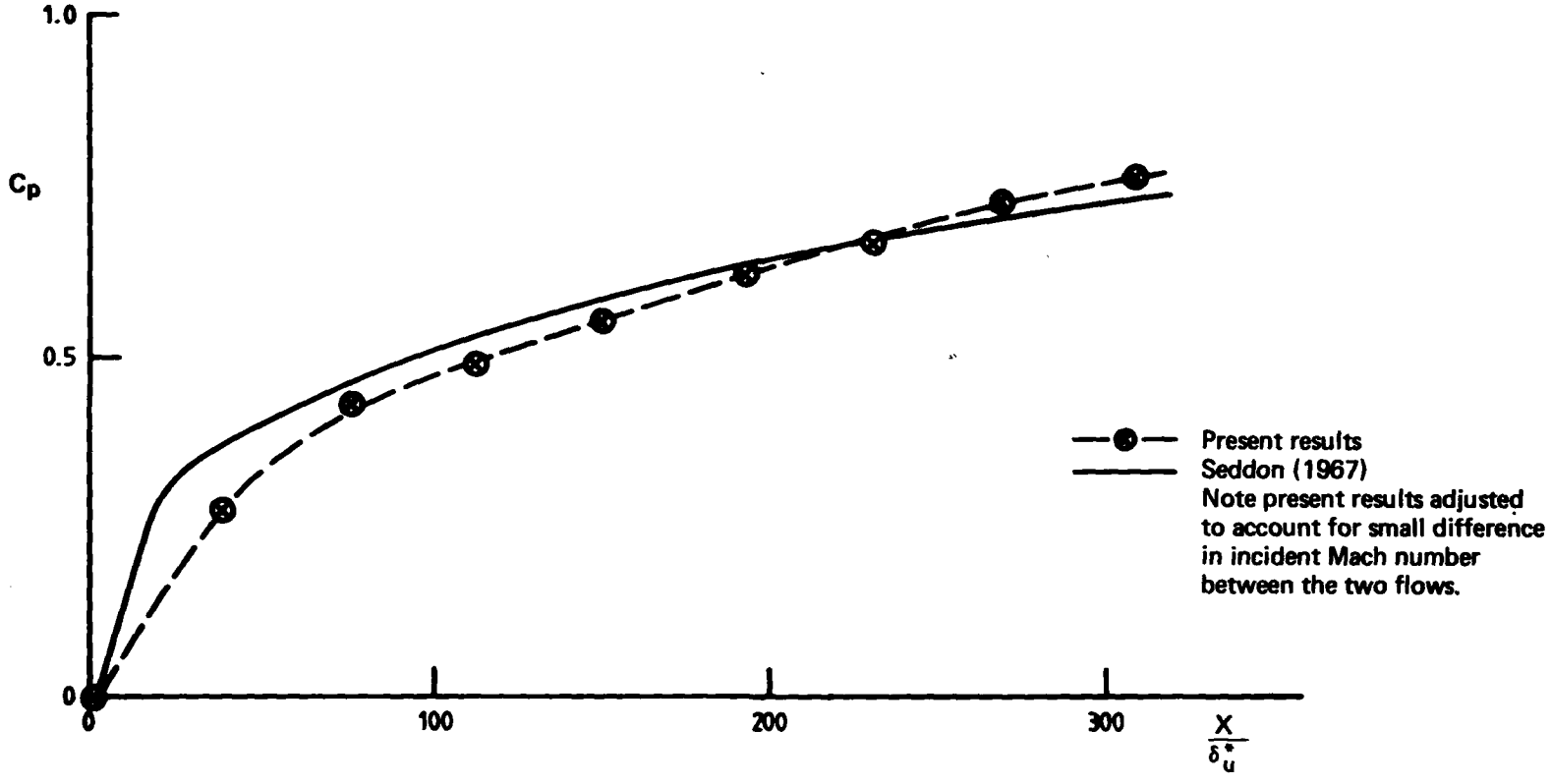

FIG. 9 WALL PRESSURE DISTRIBUTIONS NEAR SHOCK WAVE.

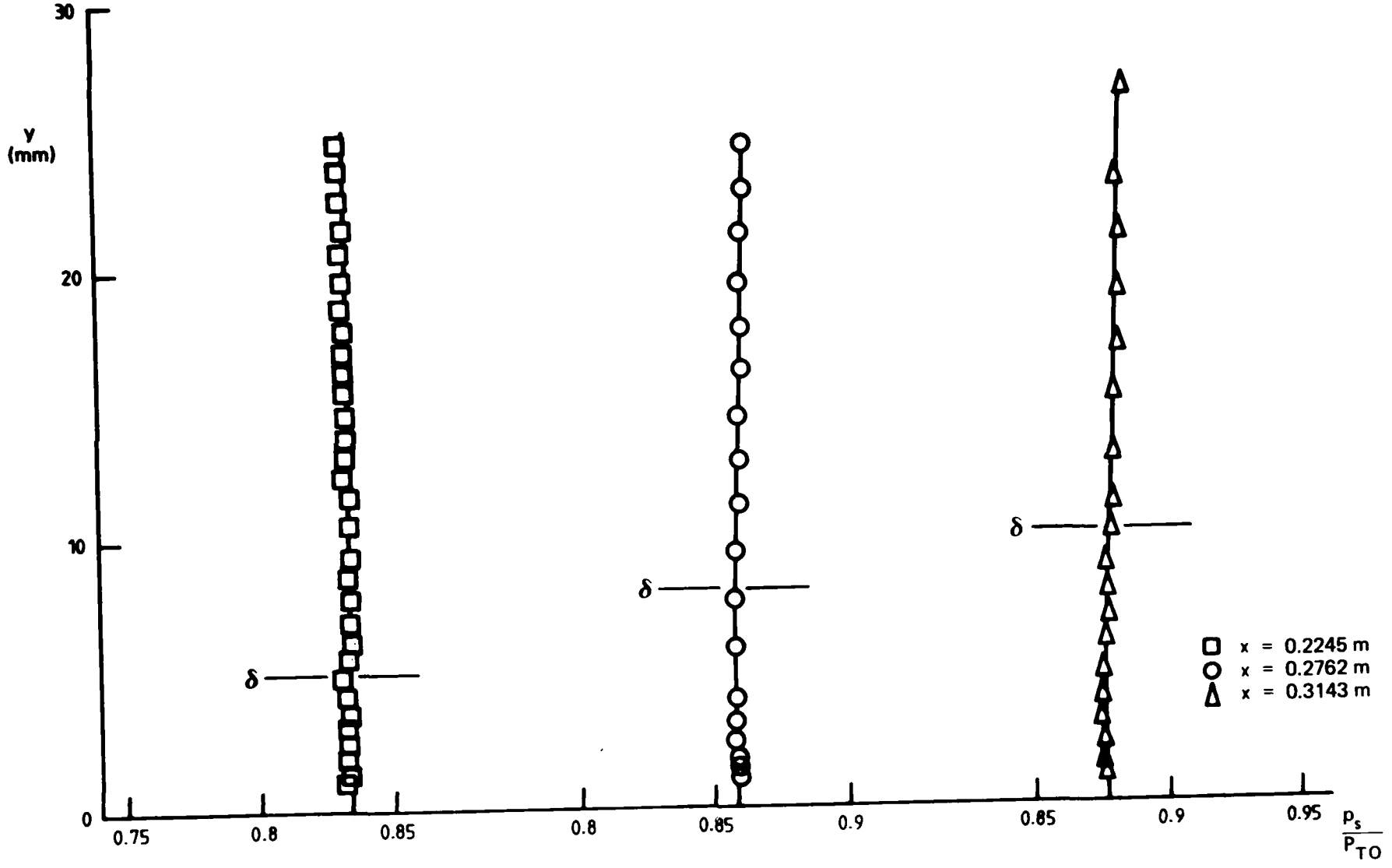

FIG. 10 STATIC PRESSURE PROFILES – LAYER L

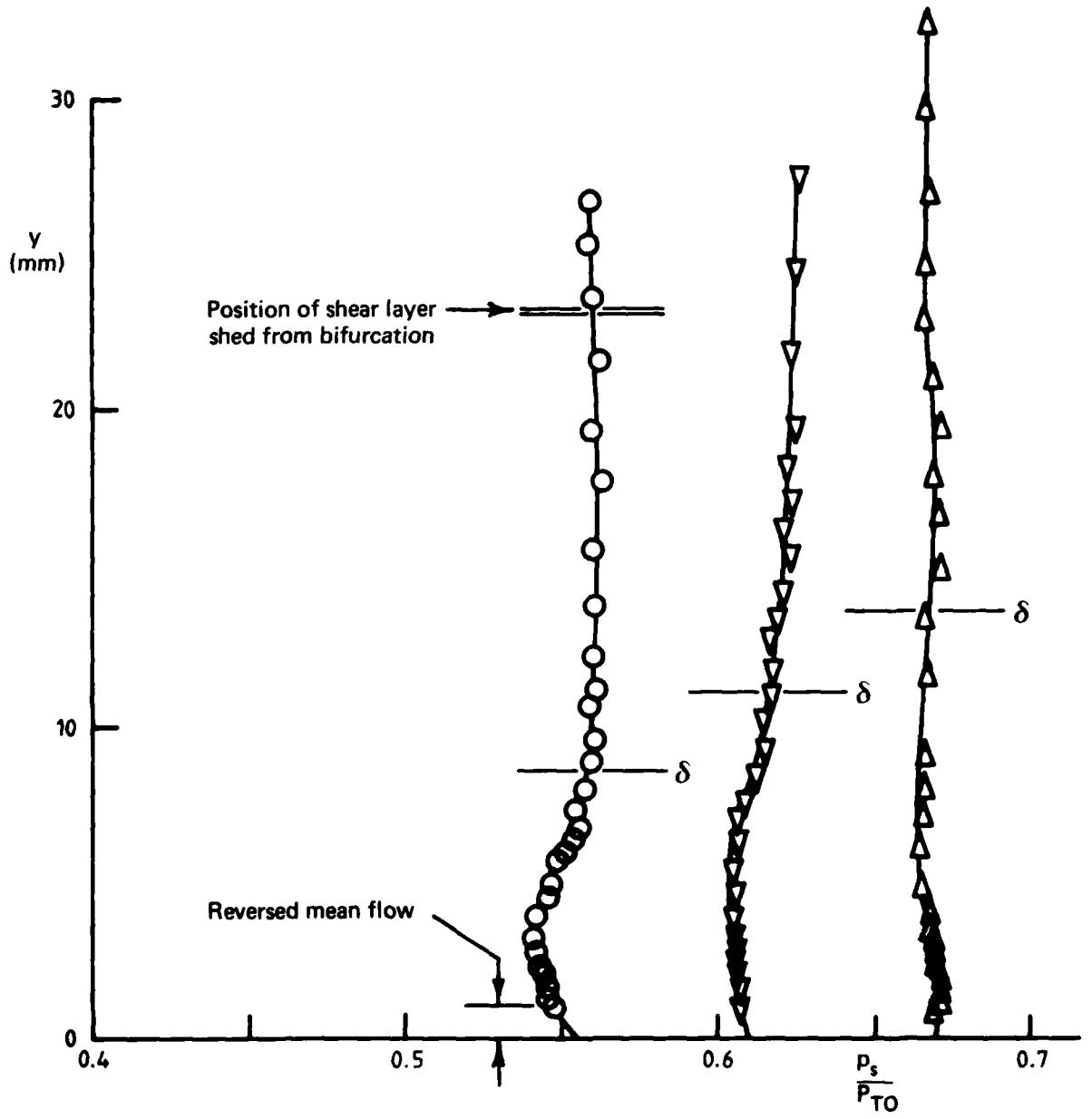

○ 0.2762m (X = 19 δ_u)

▽ 0.3143m (X = 31 δ_u)

△ 0.4031m (X = 58 δ_u) Reattachment at 0.28m

FIG. 11 STATIC PROFILES – LAYER S

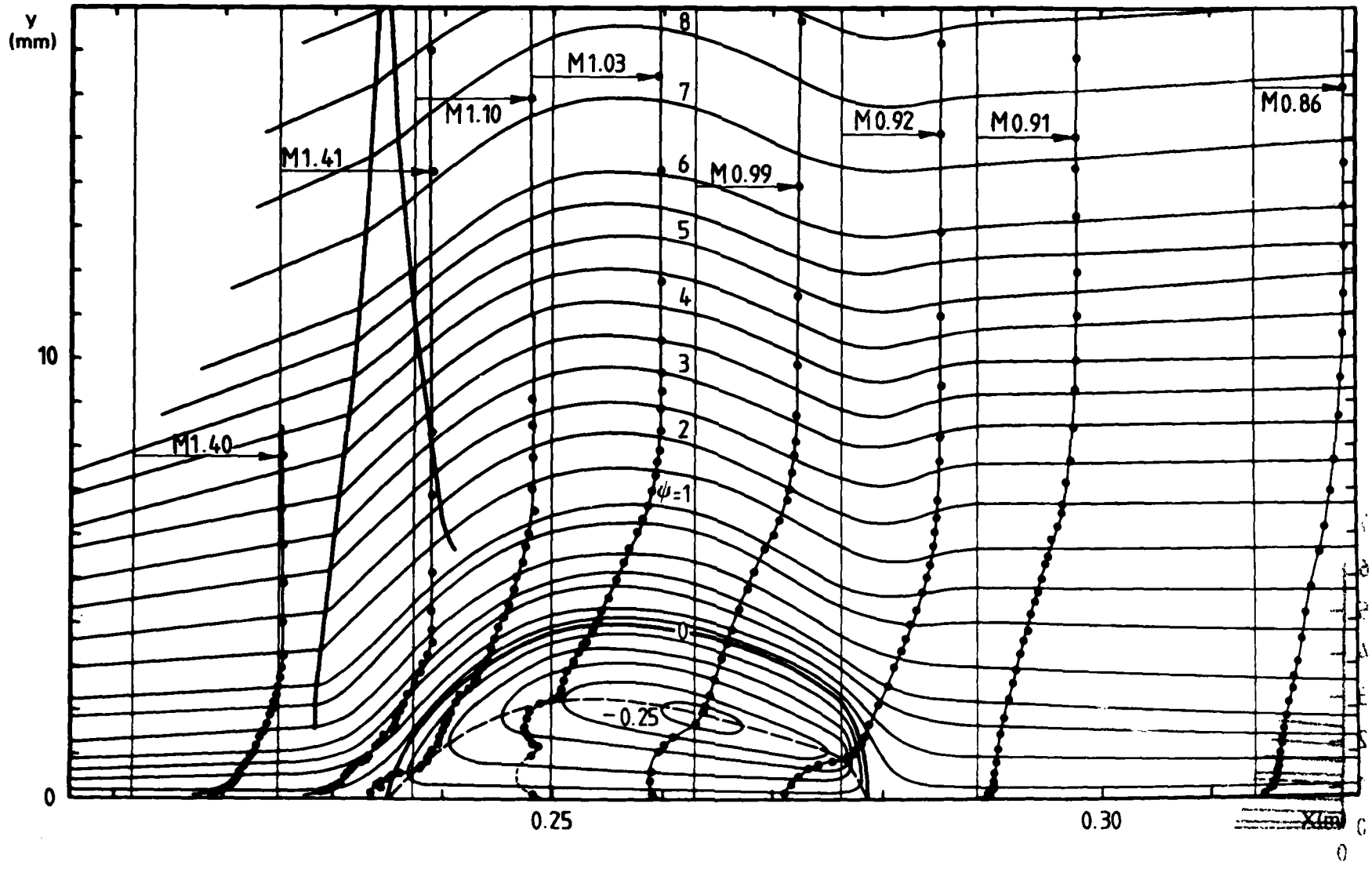

FIG. 12 MEAN STREAMLINES ON CENTRELINE IN VICINITY OF THE INTERACTION.

Note vertical scale four times larger than horizontal scale.
Units for ψ are kgm/m.s.

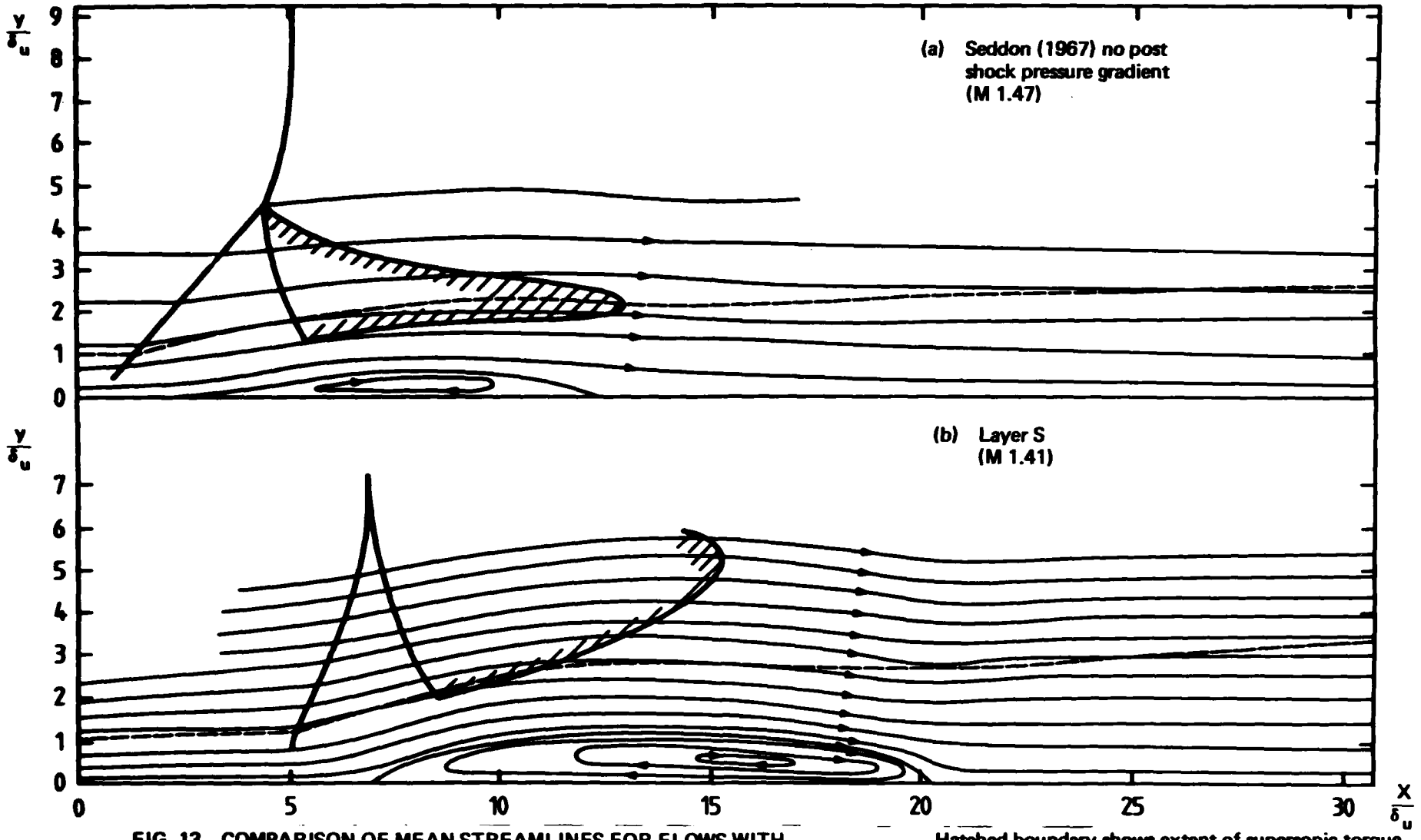

FIG. 13 COMPARISON OF MEAN STREAMLINES FOR FLOWS WITH AND WITHOUT A POST SHOCK PRESSURE GRADIENT

Hatched boundary shows extent of supersonic torque. Broken line indicates edge of boundary layer.

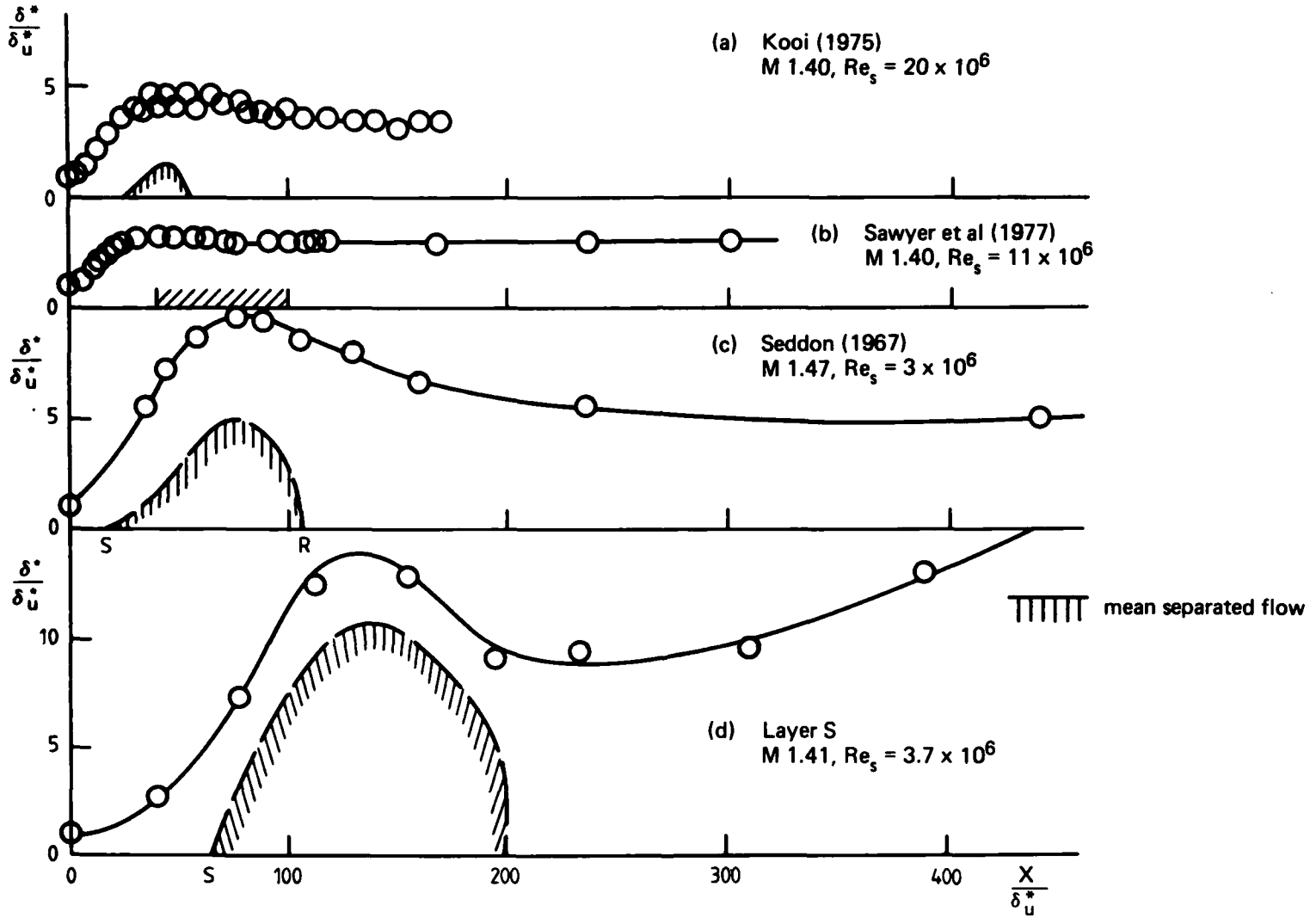

FIG. 14 DISPLACEMENT THICKNESS GROWTH THROUGH INTERACTION WITH AND WITHOUT POST SHOCK PRESSURE GRADIENT.

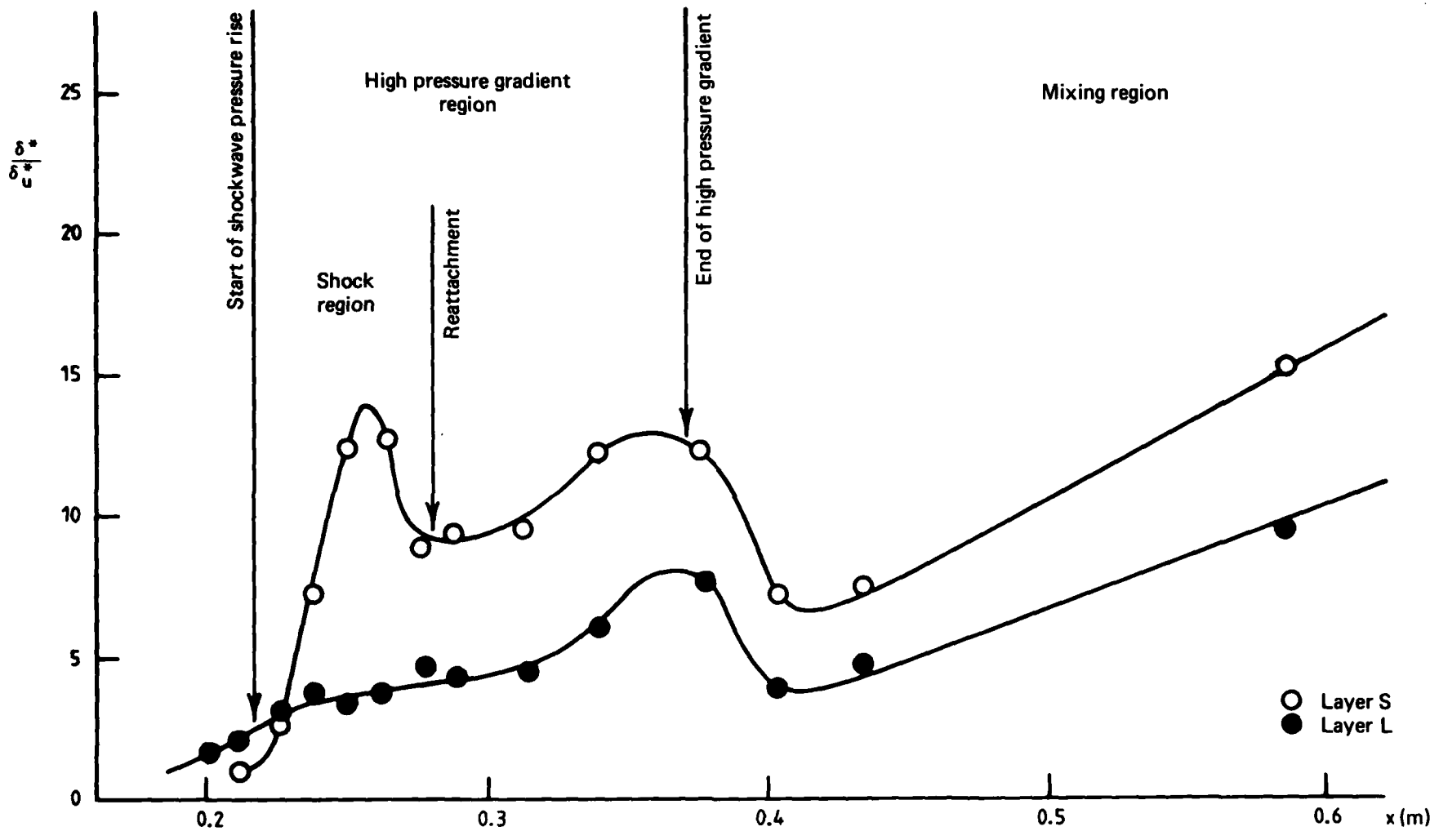

FIG. 15 DISPLACEMENT THICKNESS GROWTH WITH AND WITHOUT A SHOCK WAVE – HIGH PRESSURE GRADIENT REGION.

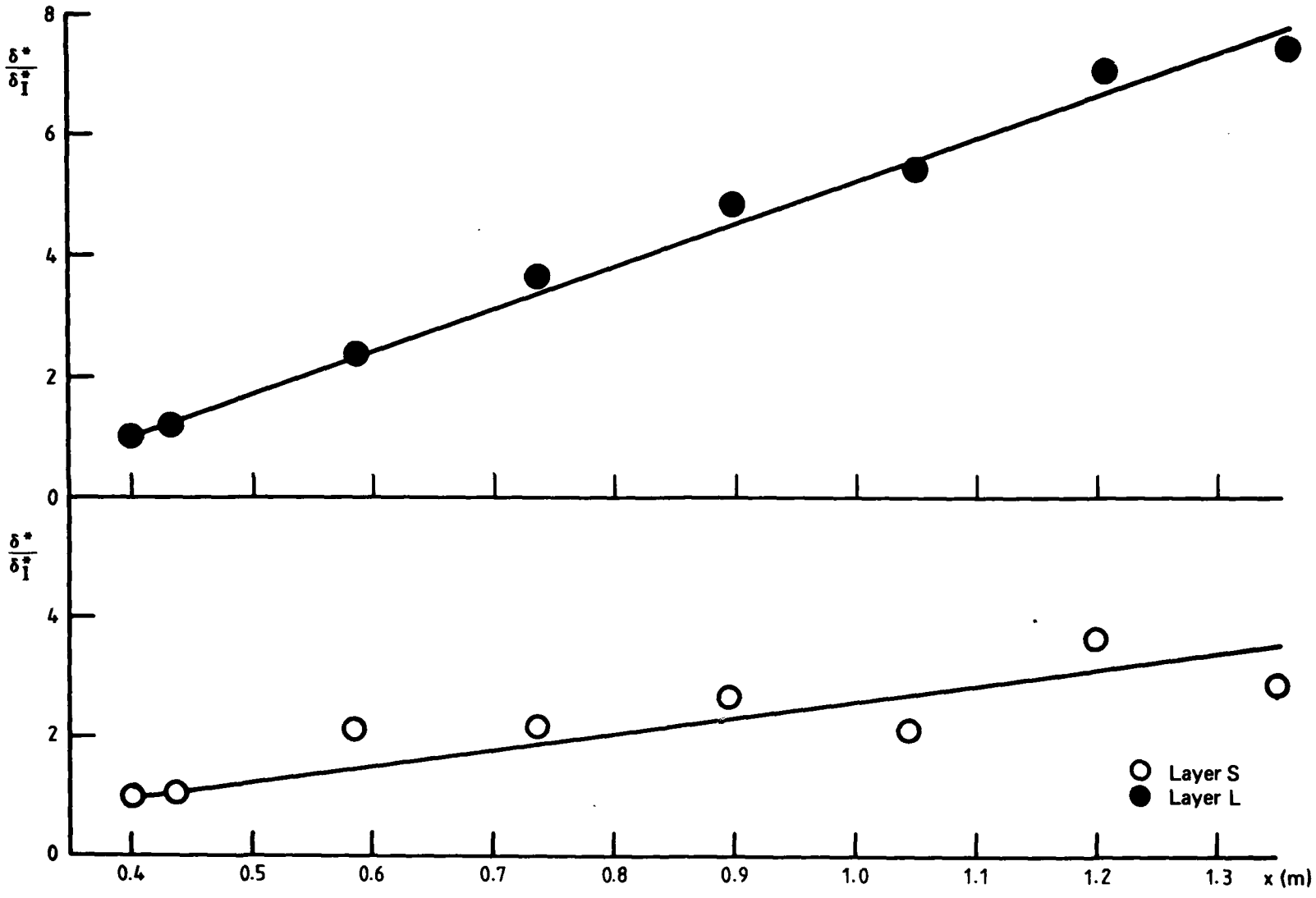

FIG. 16 DISPLACEMENT THICKNESS GROWTH IN THE MIXING REGION WITH AND WITHOUT A SHOCK WAVE.

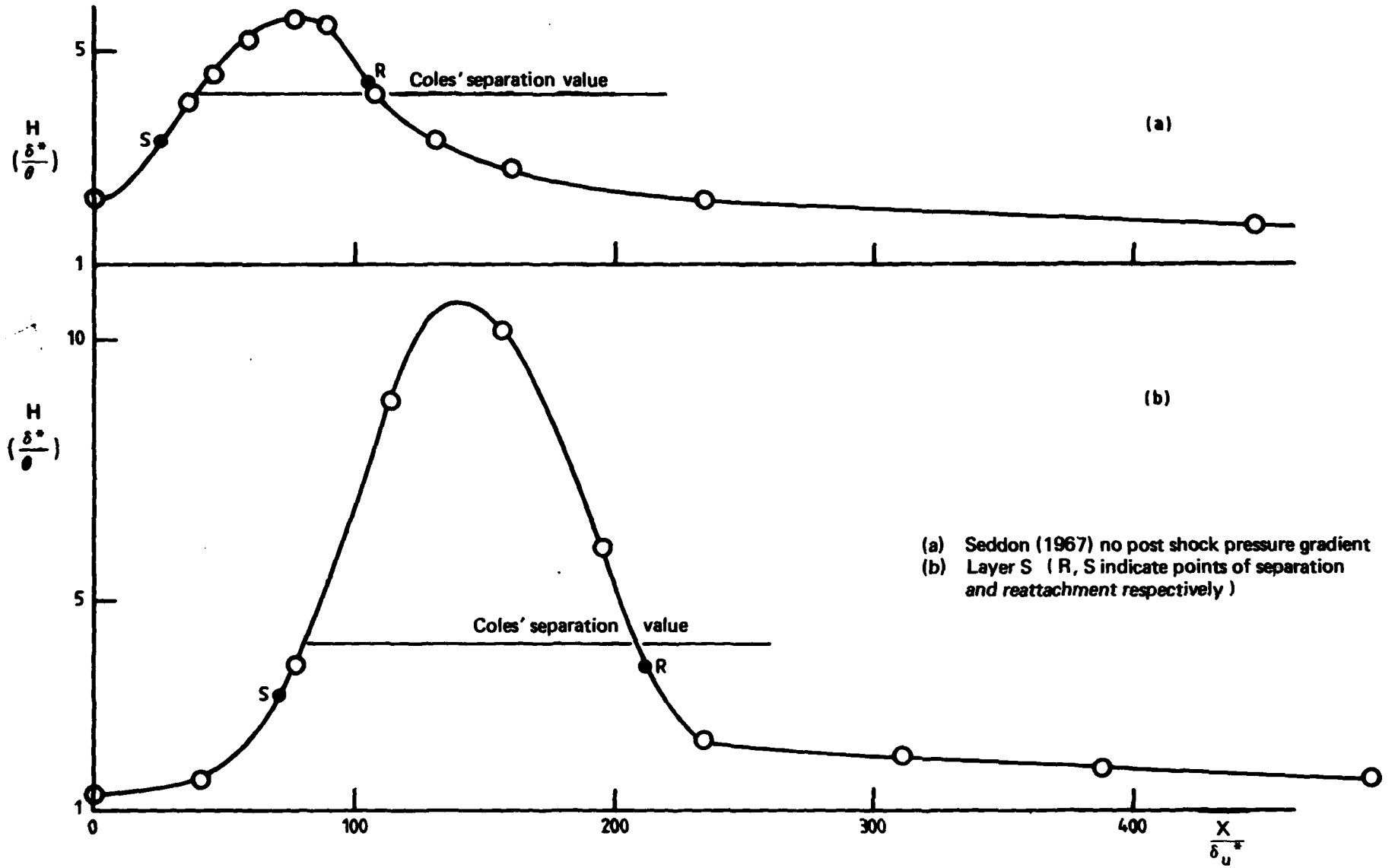

FIG. 17 SHAPE FACTOR VARIATION IN THE REGION NEAR THE SHOCK WAVE.

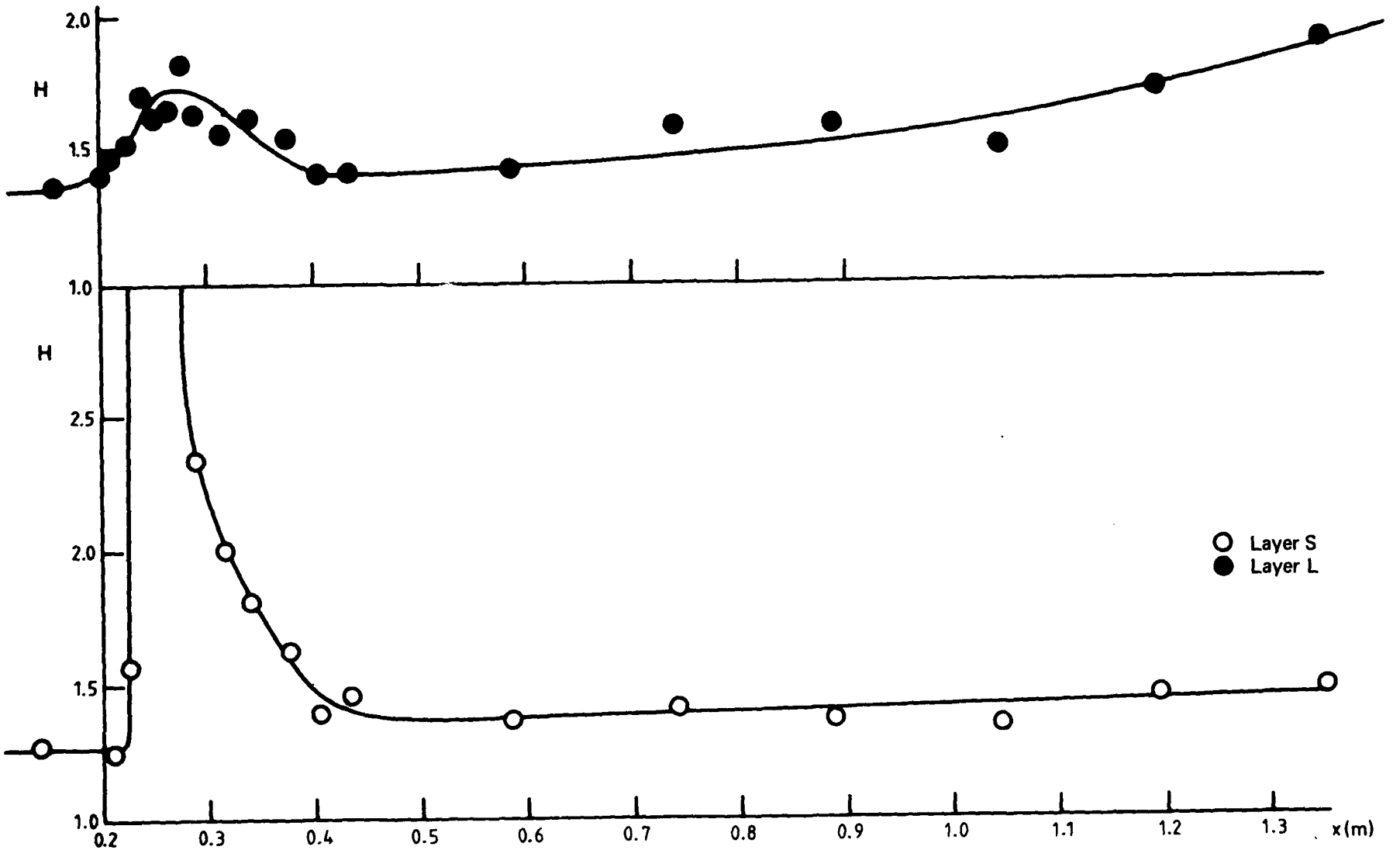

FIG. 18 SHAPE FACTOR VARIATION

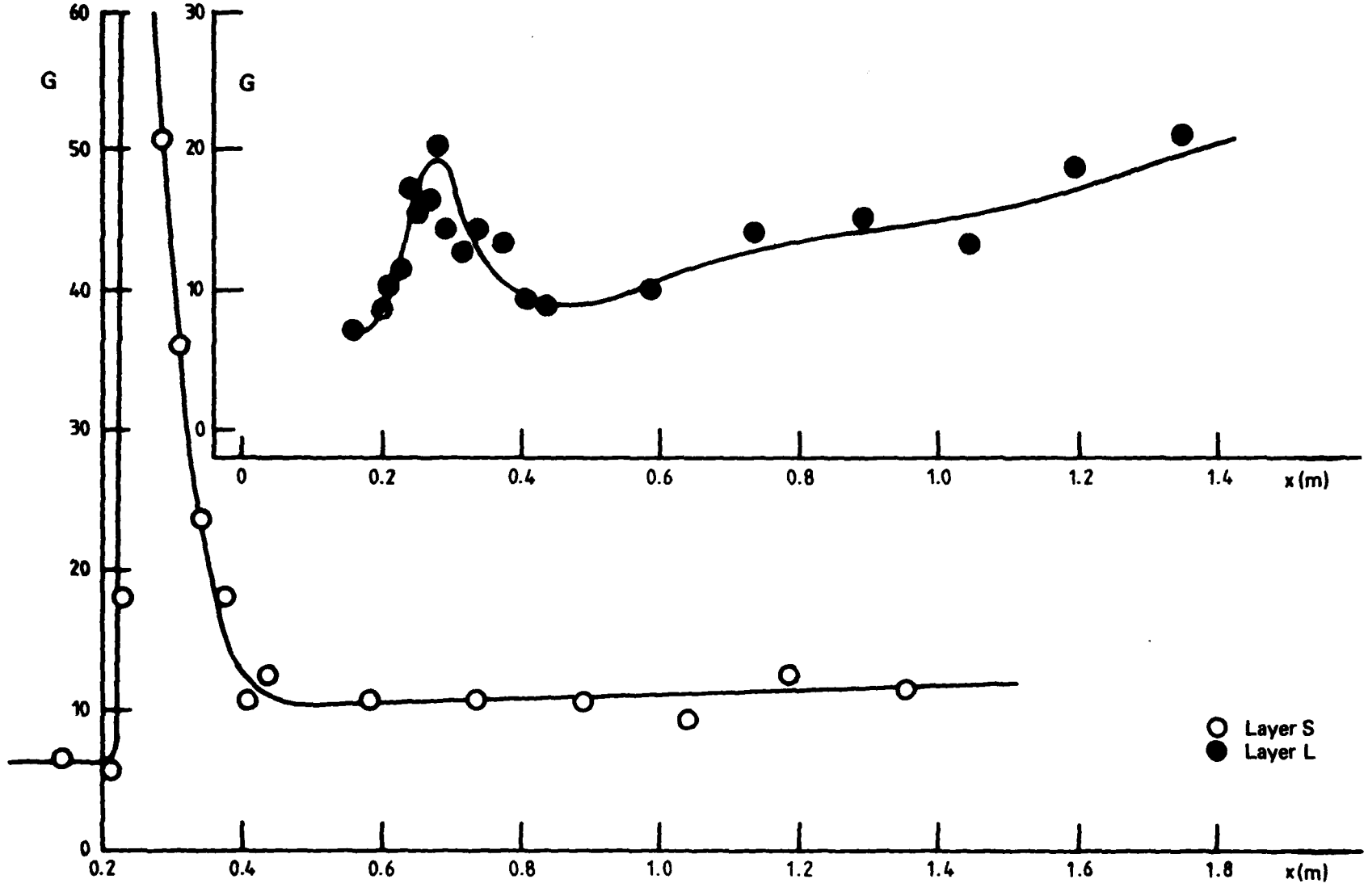

FIG. 19 CLAUSER'S SHAPE FACTOR

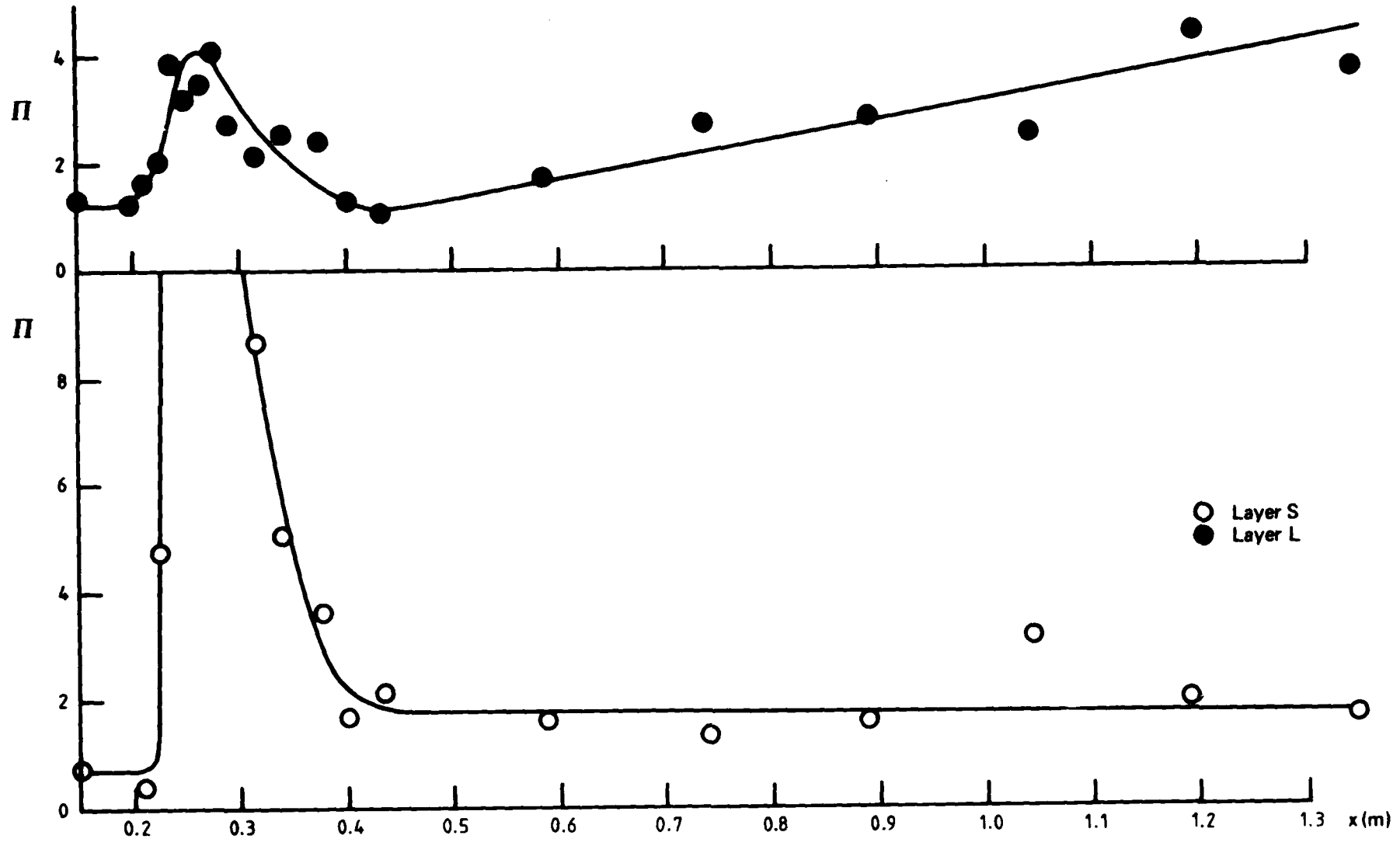

FIG. 20 COLES'WAKE STRENGTH FACTOR

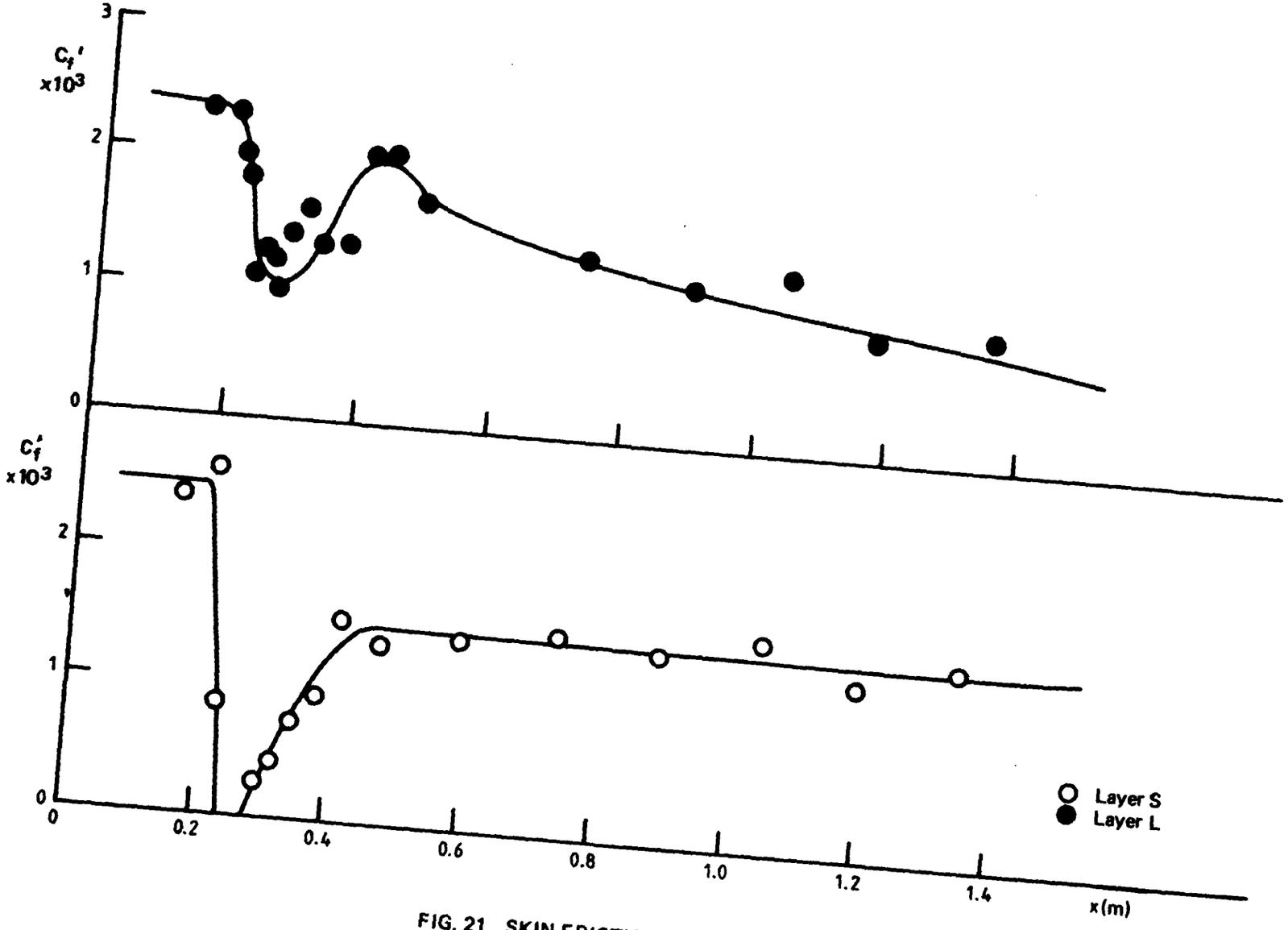

FIG. 21 SKIN FRICTION VARIATION

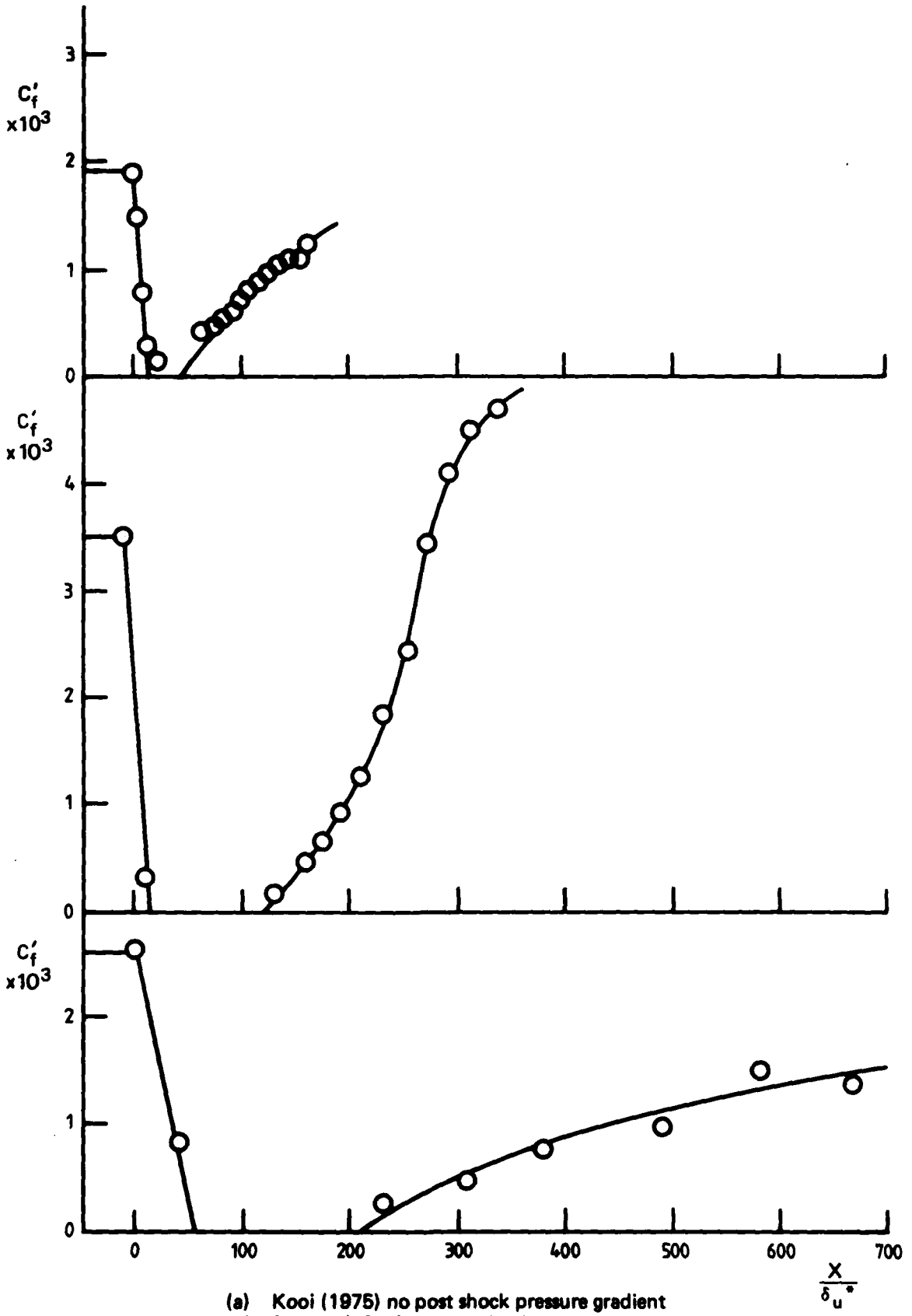

(a) Kooi (1975) no post shock pressure gradient
(b) Seddon (1967) no post shock pressure gradient
(c) Present results Layer S

FIG. 22 SKIN FRICTION VARIATION IN THE REGION NEAR A SHOCK WAVE.

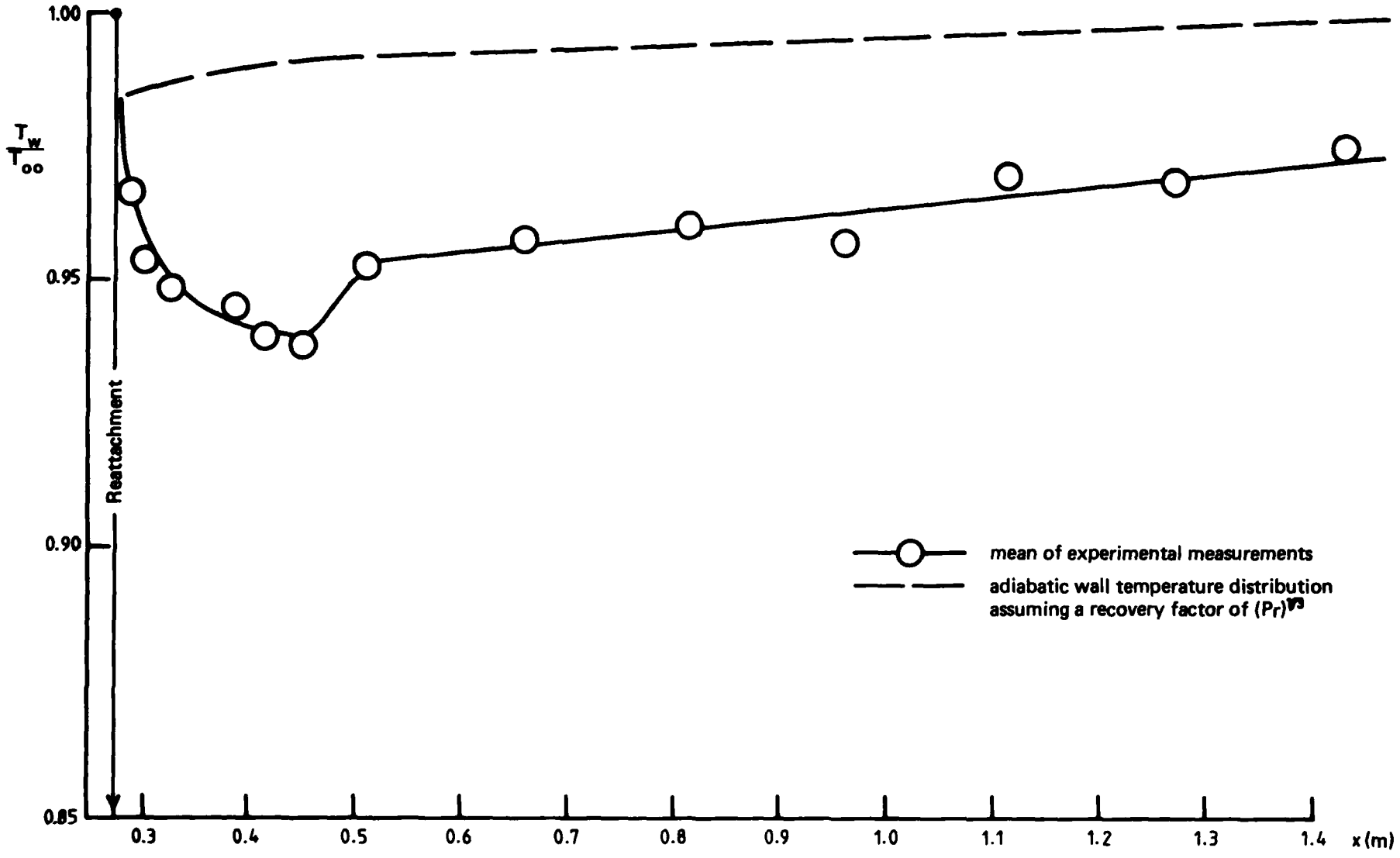

FIG. 23 WALL TEMPERATURE DISTRIBUTION – LAYER S

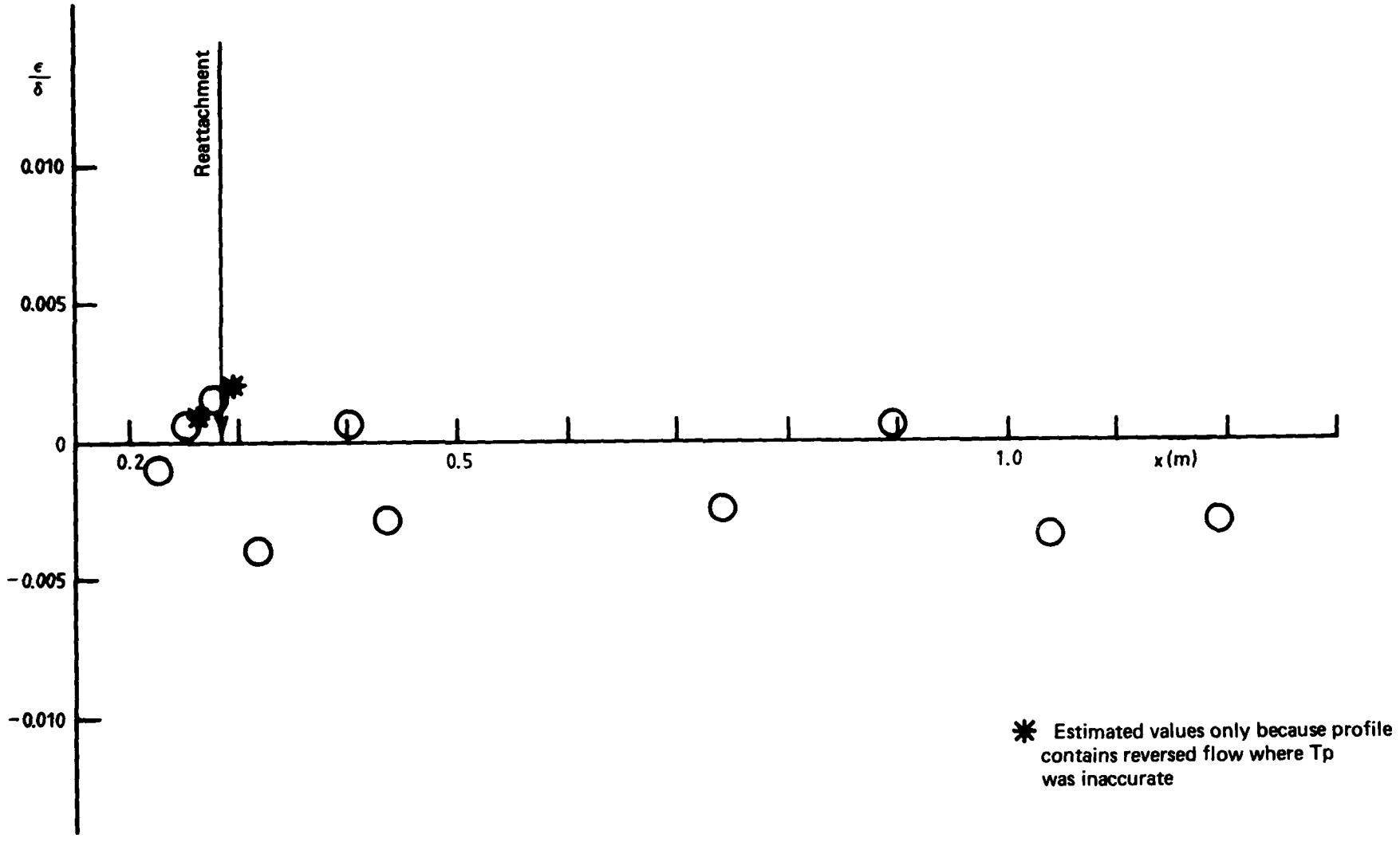

FIG. 24 ENTHALPY THICKNESS DISTRIBUTION – LAYER S

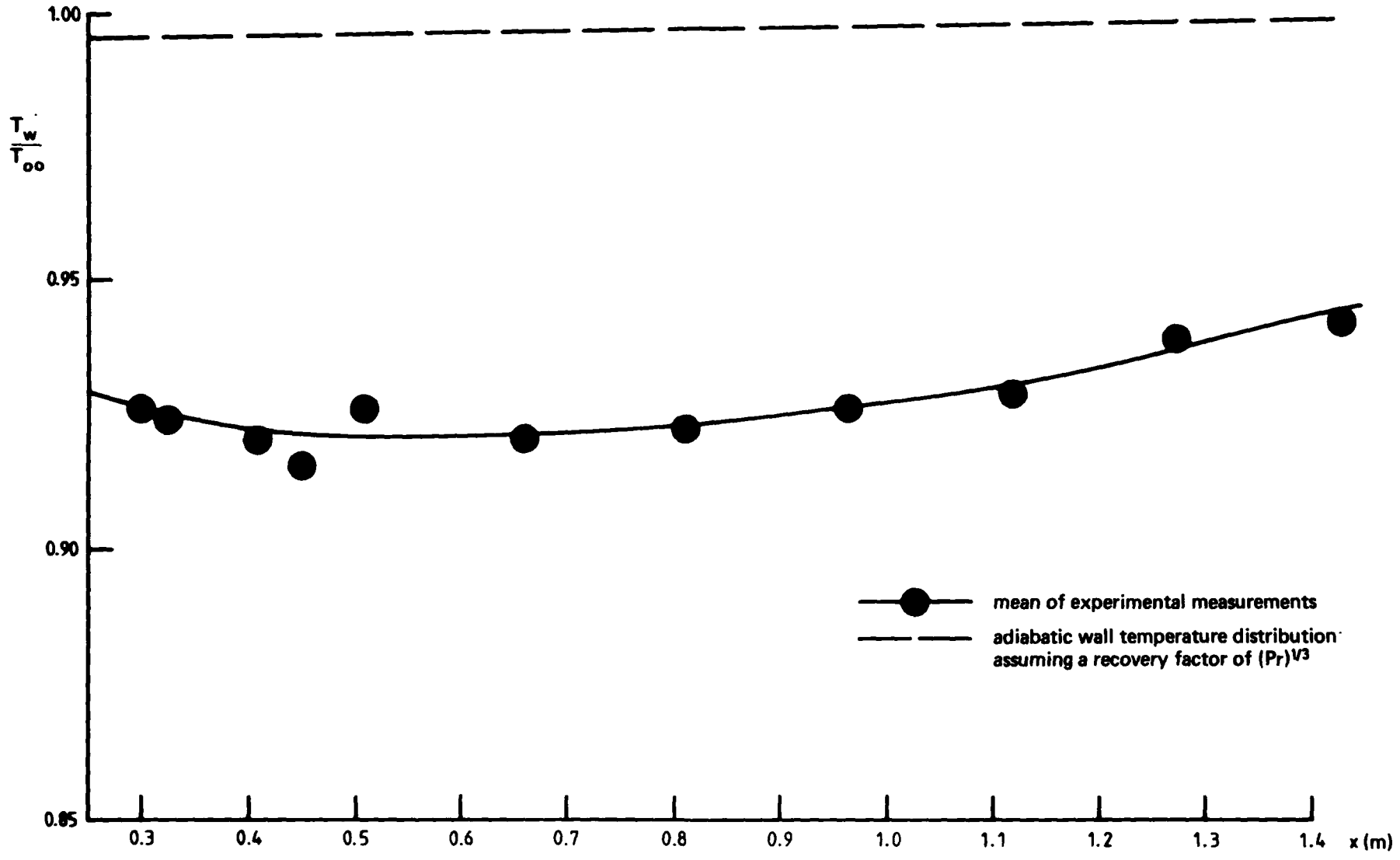

FIG. 25 WALL TEMPERATURE DISTRIBUTION – LAYER L

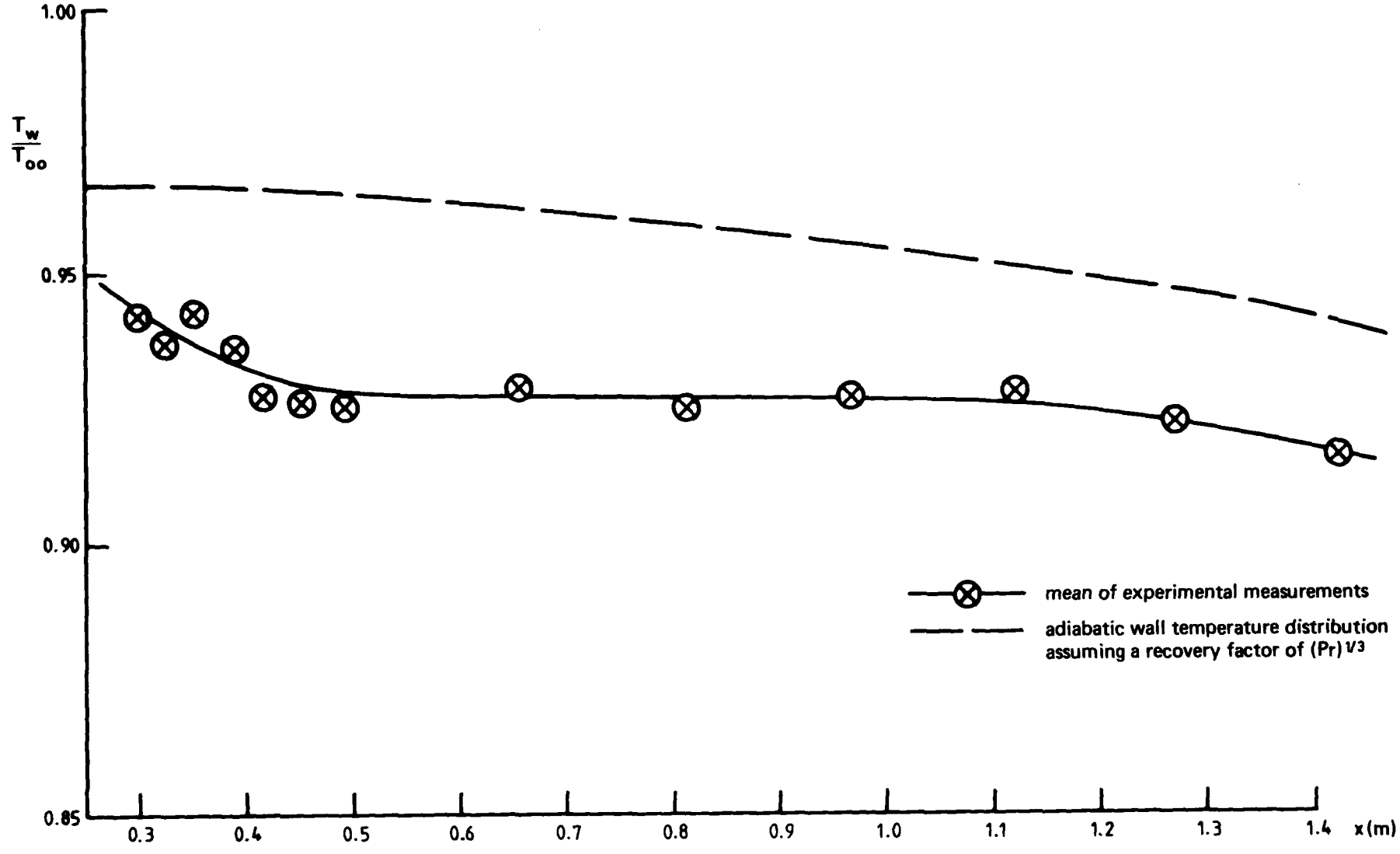

FIG. 26 WALL TEMPERATURE DISTRIBUTION – SUPERSONIC FLOW IN FAVOURABLE PRESSURE GRADIENT.

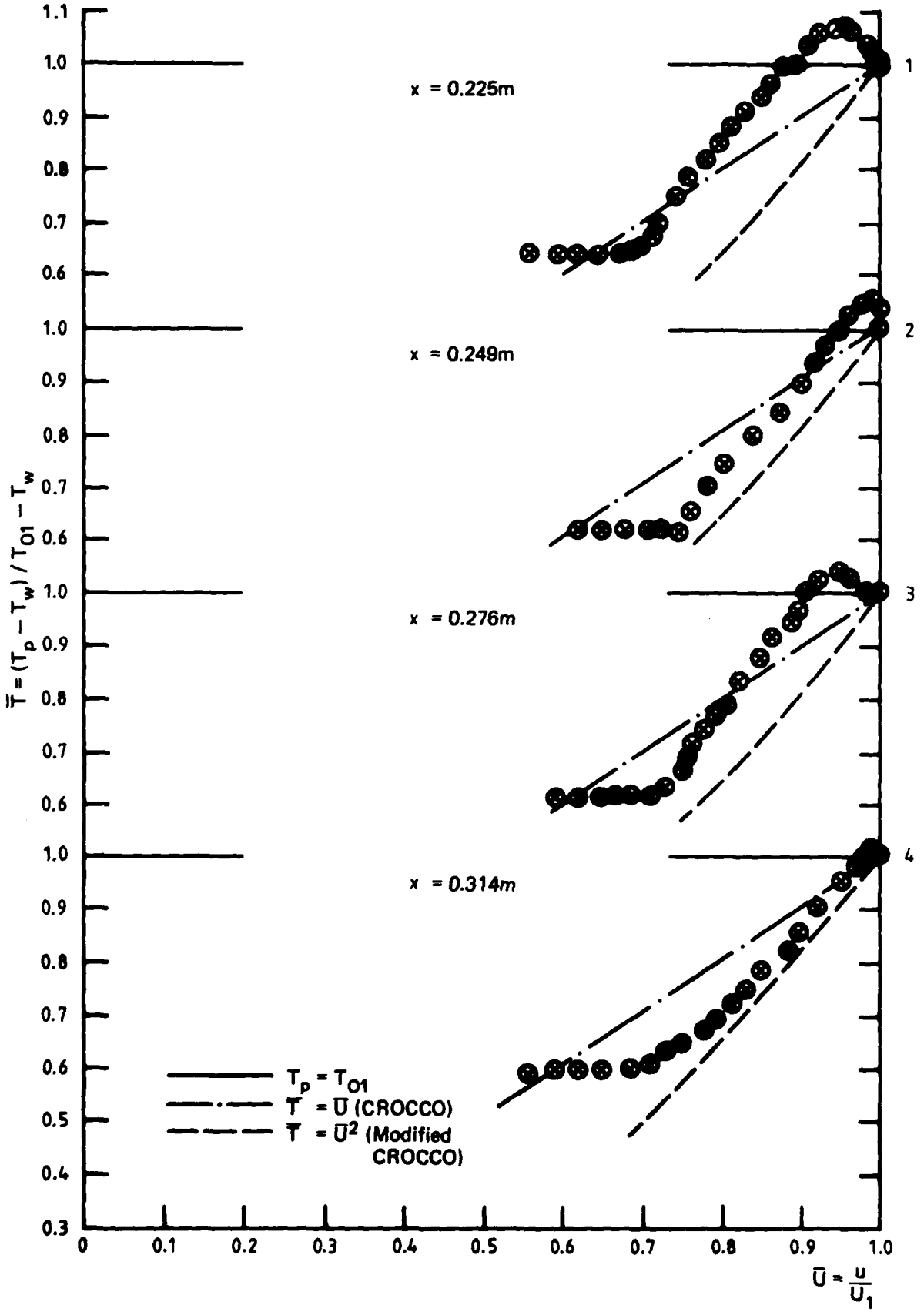

FIG. 27 TEMPERATURE PROFILES – SUPERSONIC FLOW IN FAVOURABLE PRESSURE GRADIENT.

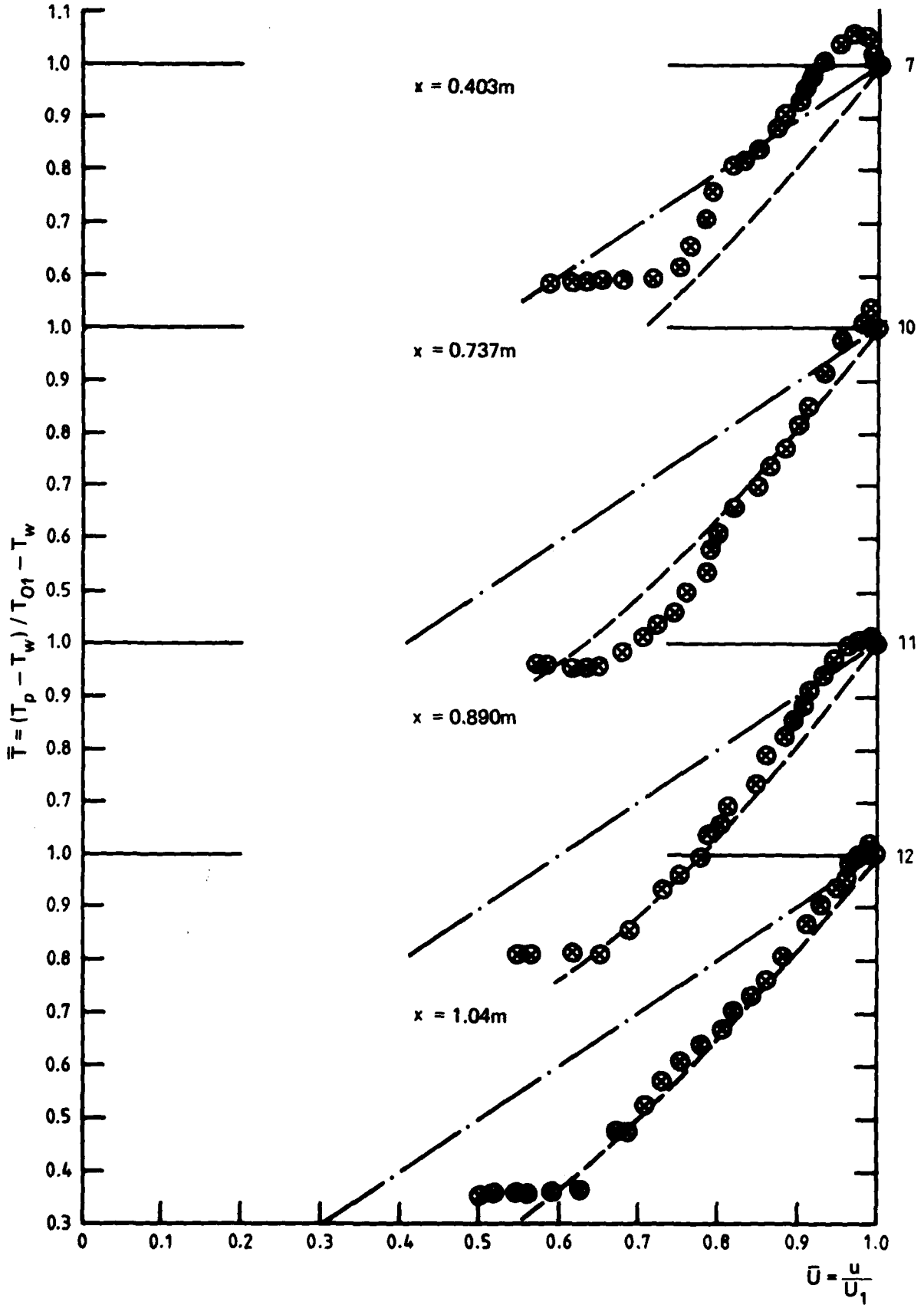

FIG. 27 (Continued)

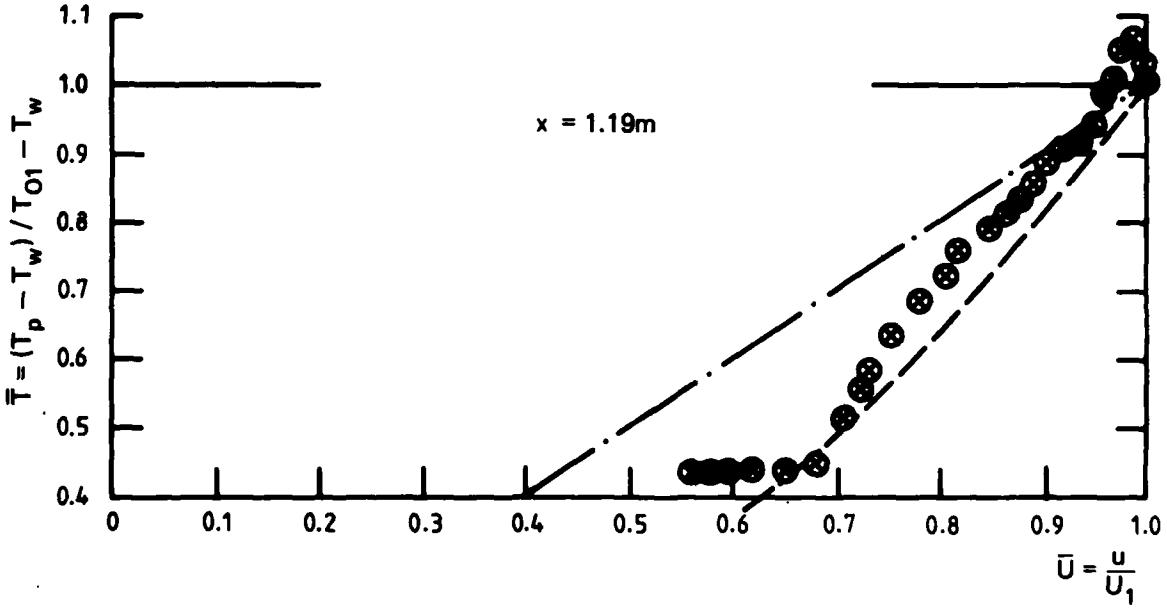

FIG. 27 (Concluded)

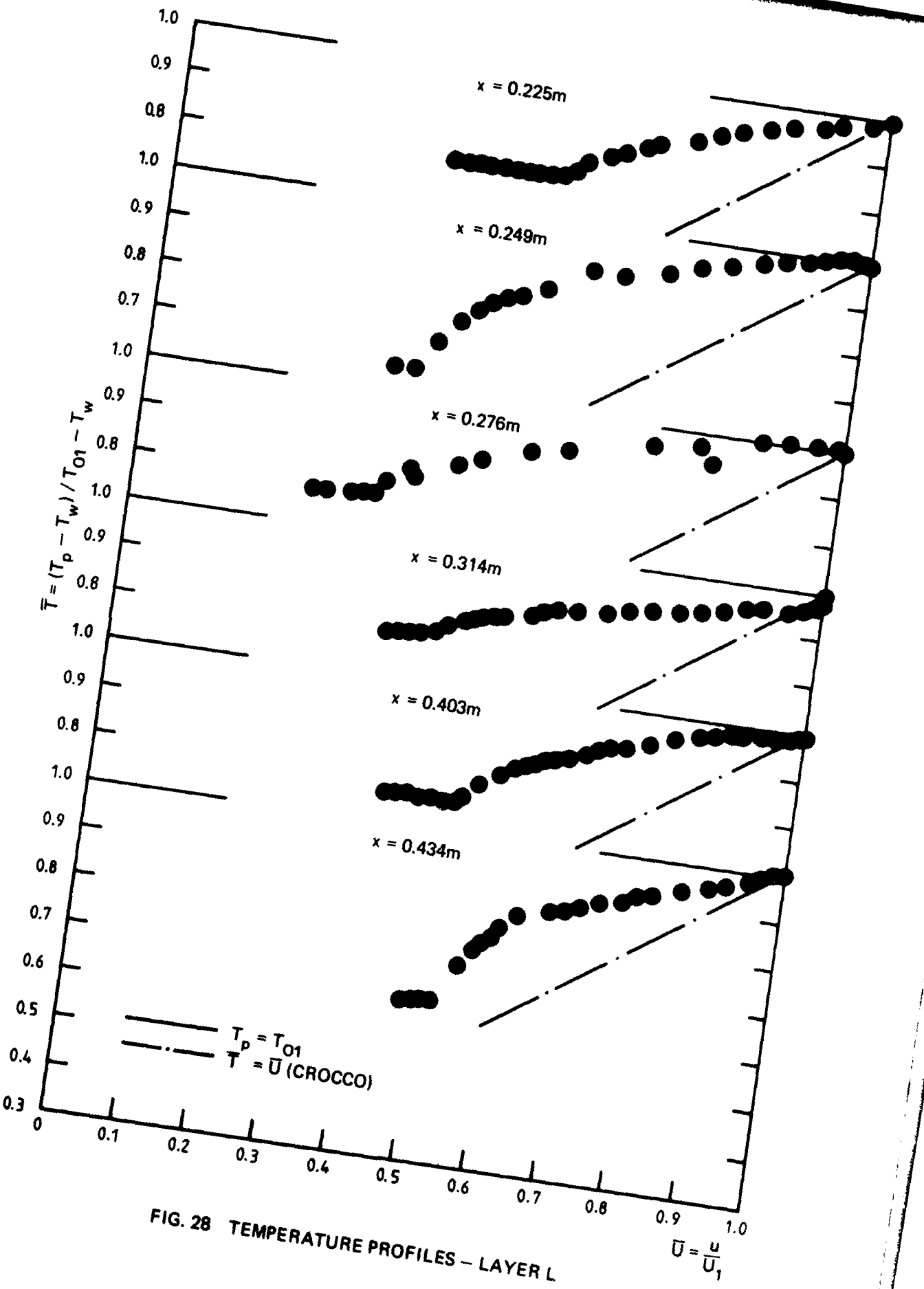

FIG. 28 TEMPERATURE PROFILES – LAYER L

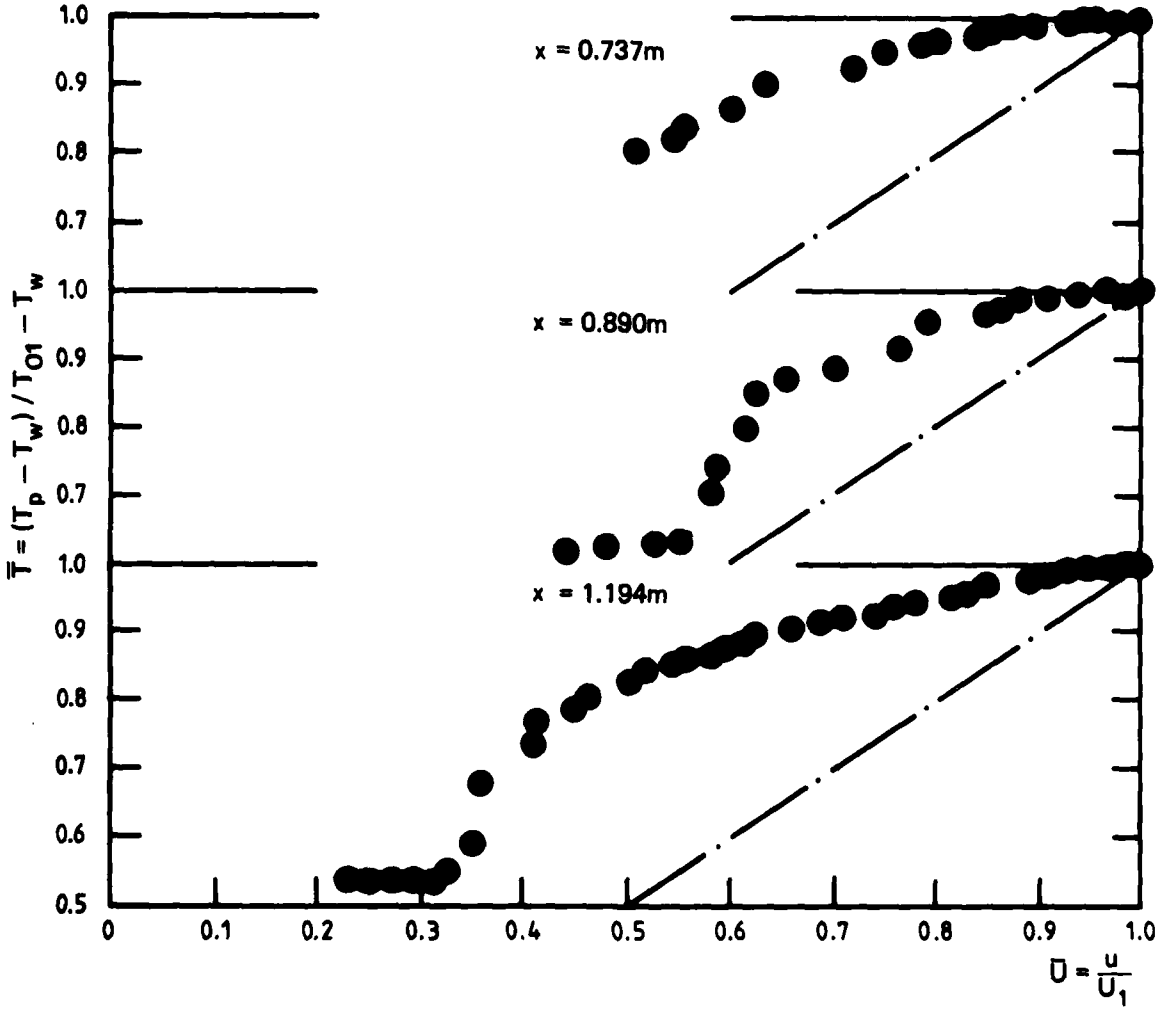

FIG. 28 (Concluded)

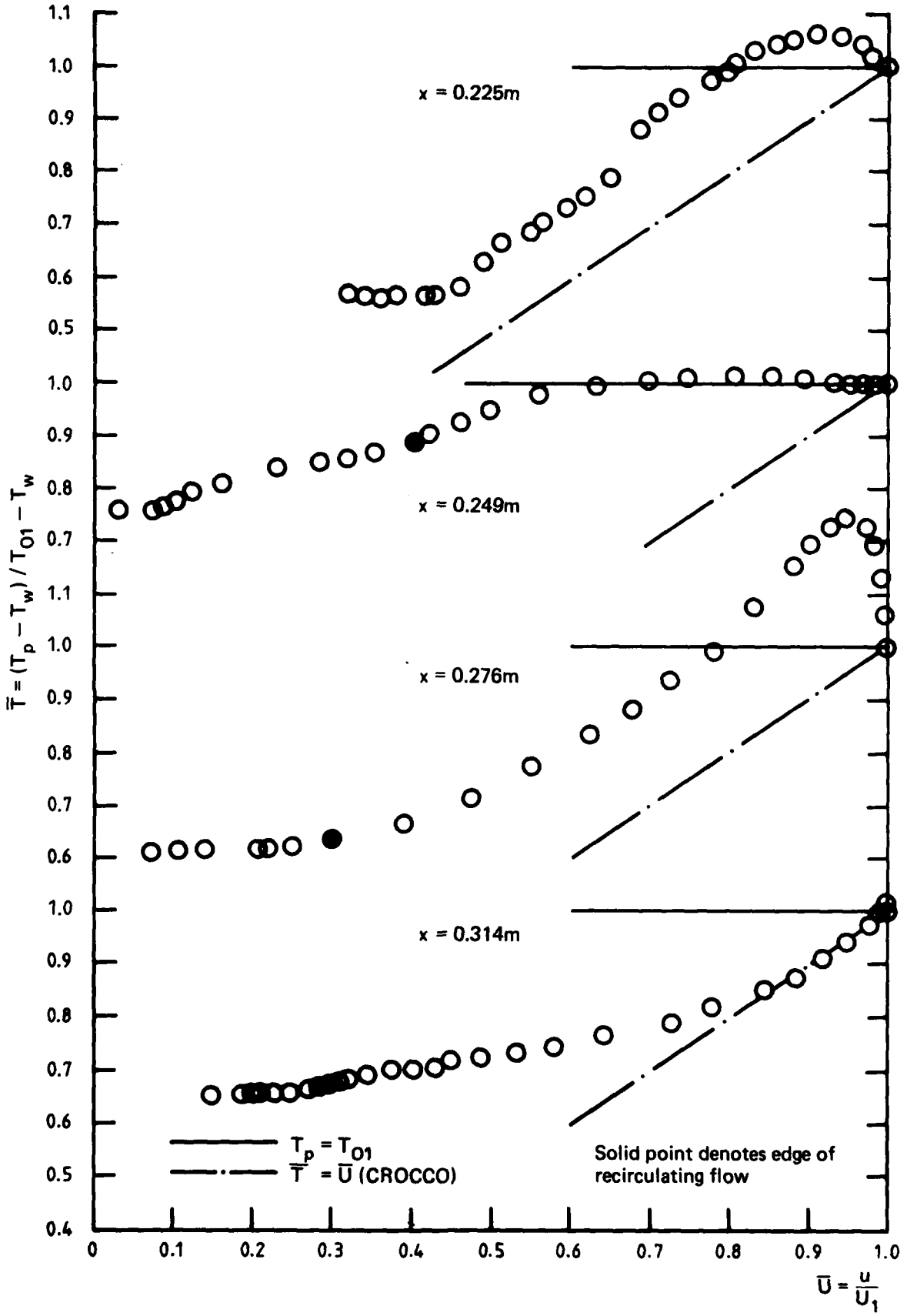

FIG. 29 TEMPERATURE PROFILES – LAYER S

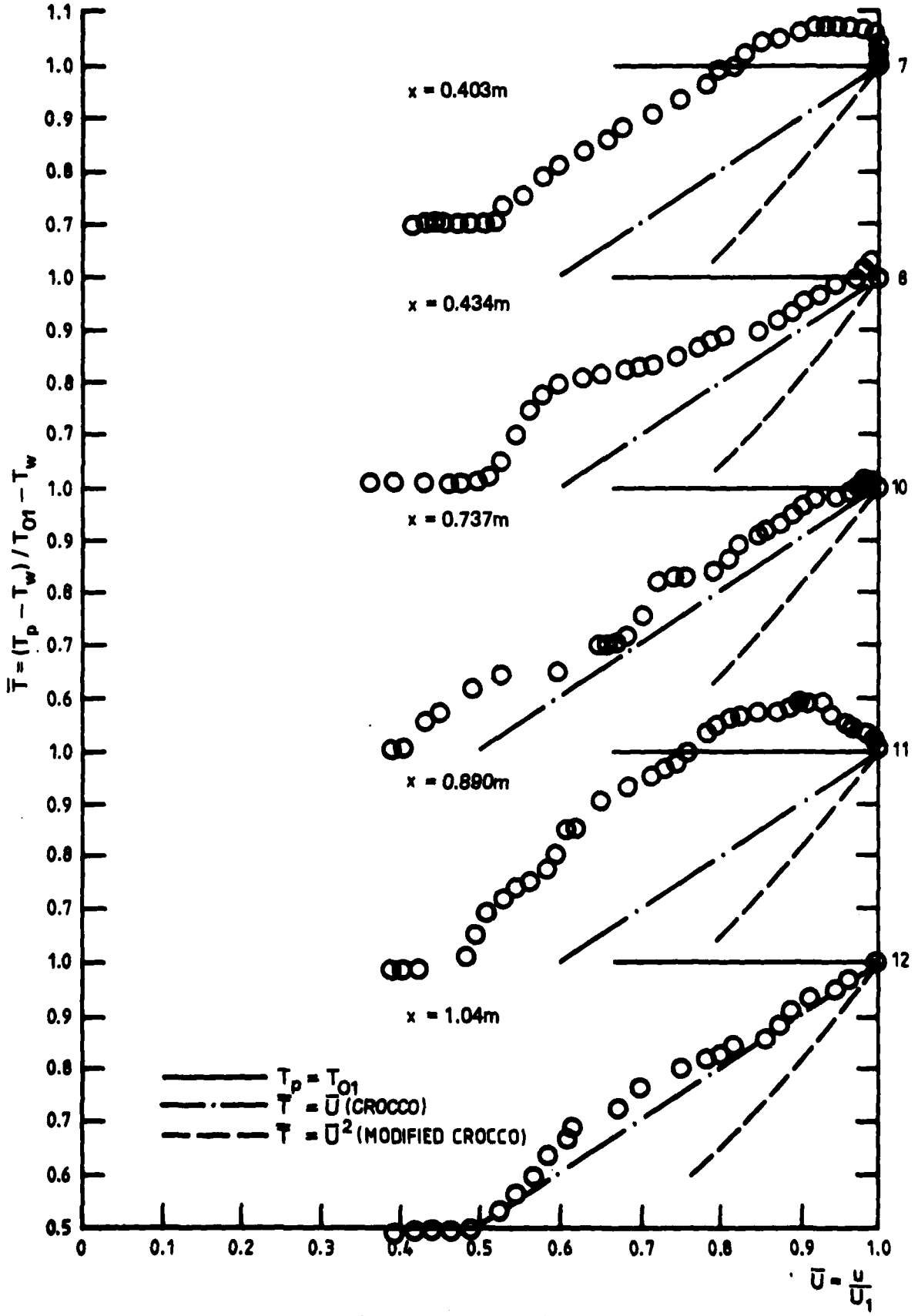

FIG. 29 (Continued)

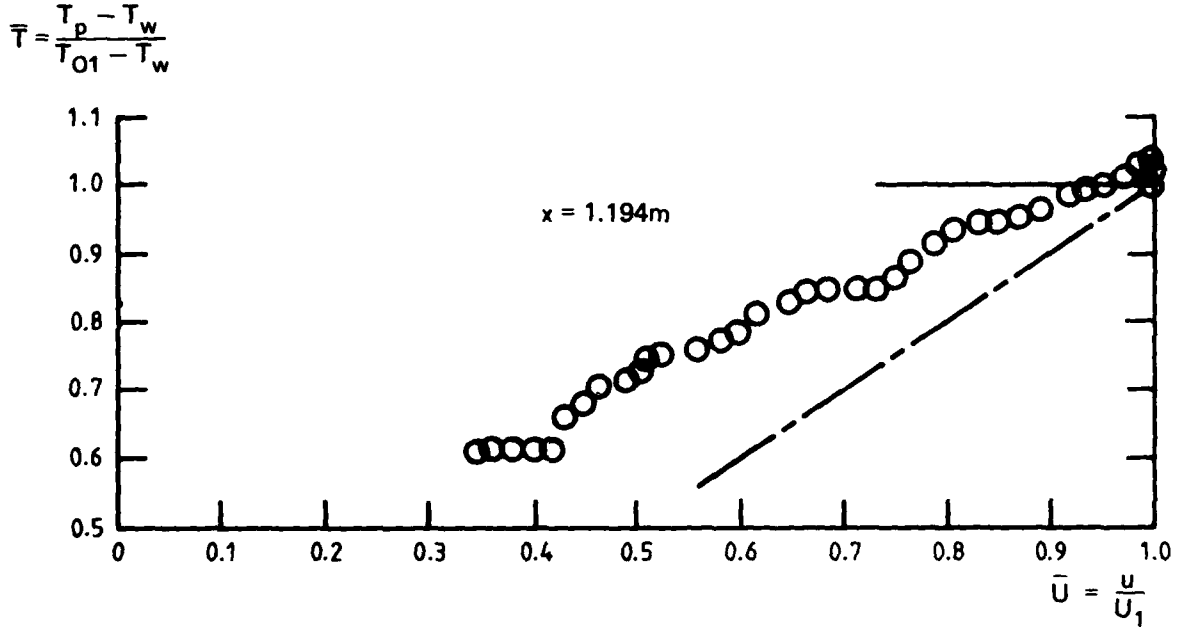

FIG. 29 (Concluded)

APPENDIX

Mean Velocity Profiles—Plotted on Wall Similarity Co-ordinates, u/U_1 versus $\log_{10} y\ U_1/\nu$.

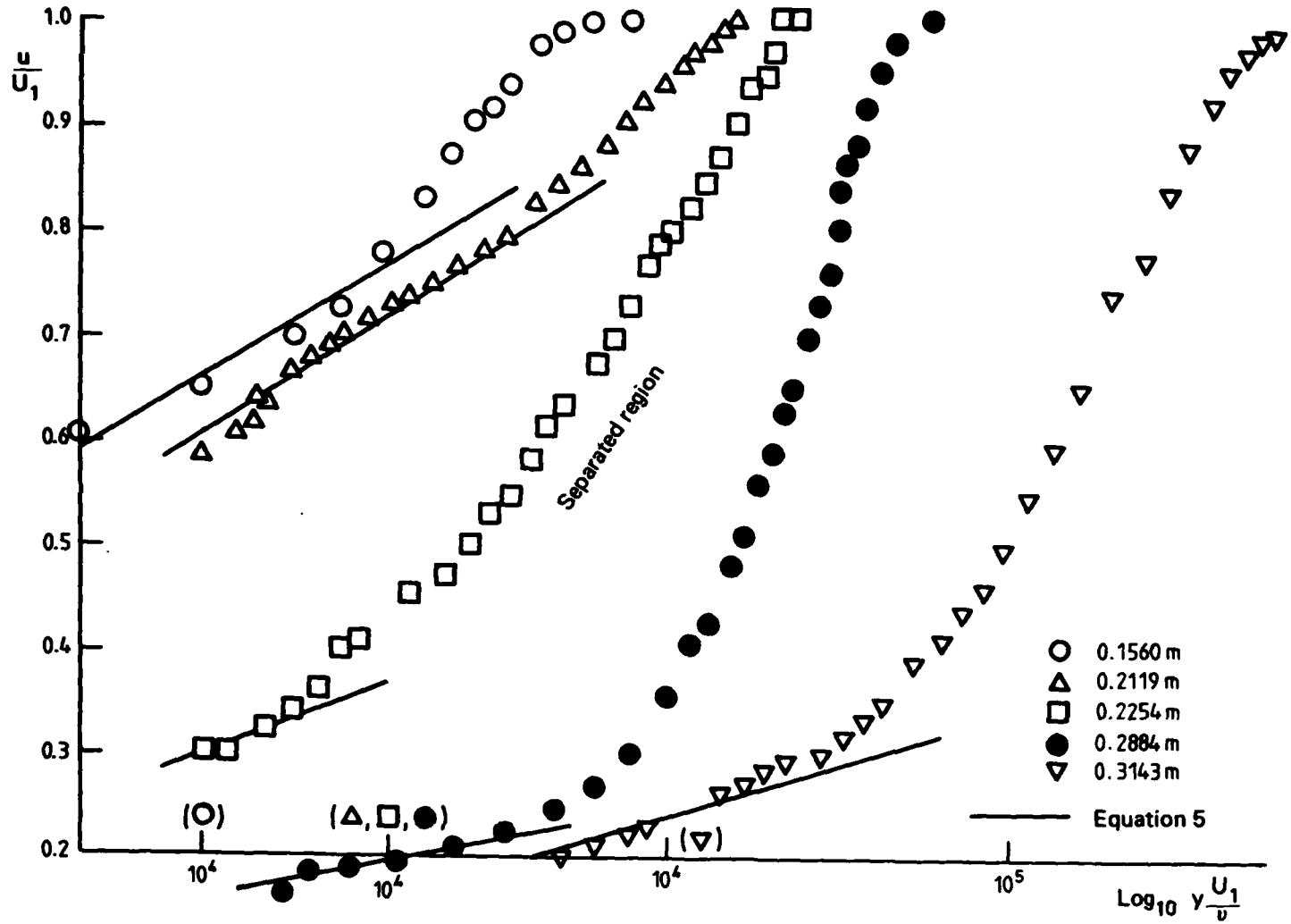

FIG. A1 -- SERIES S

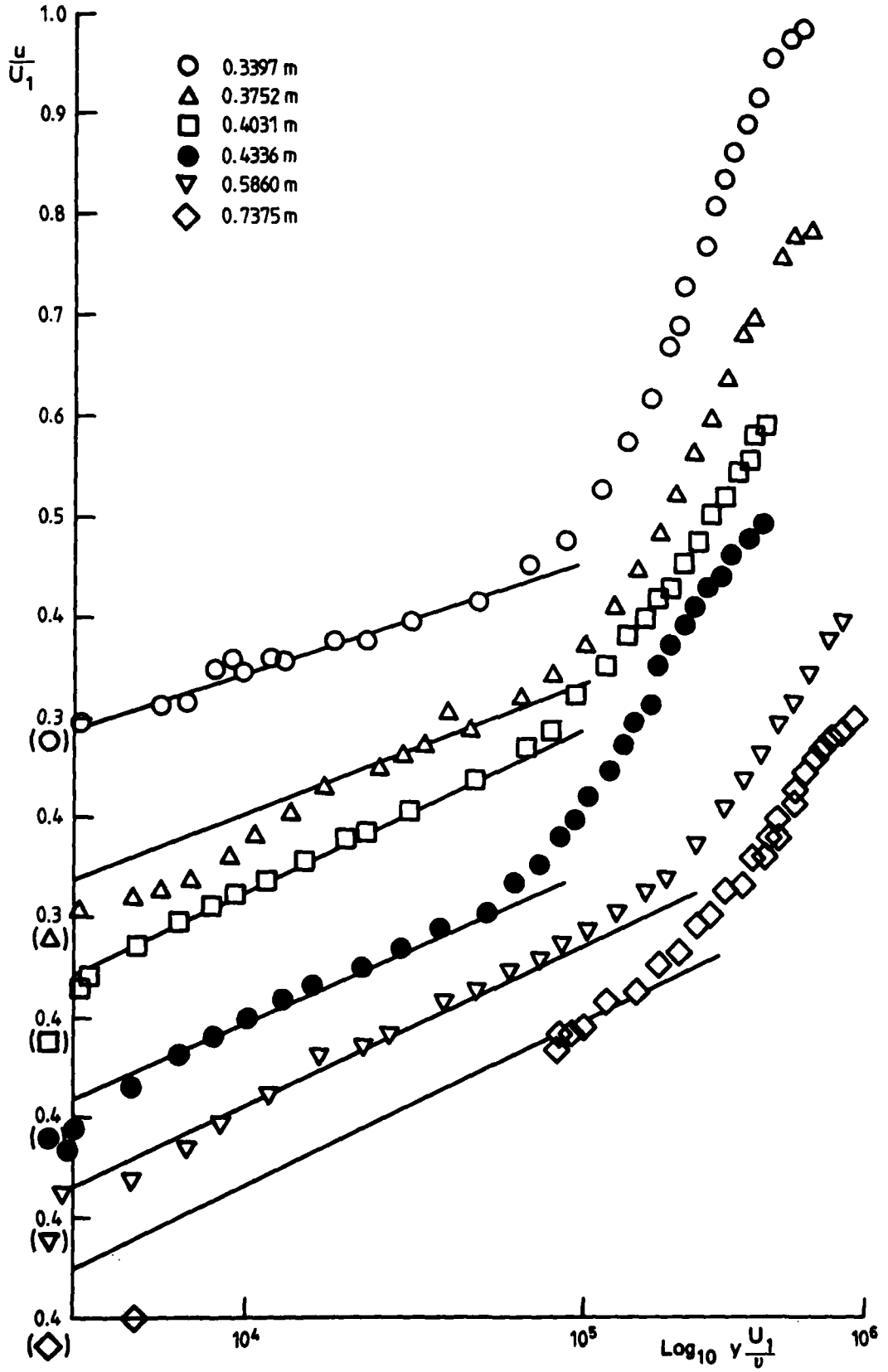

FIG. A1 (Continued)

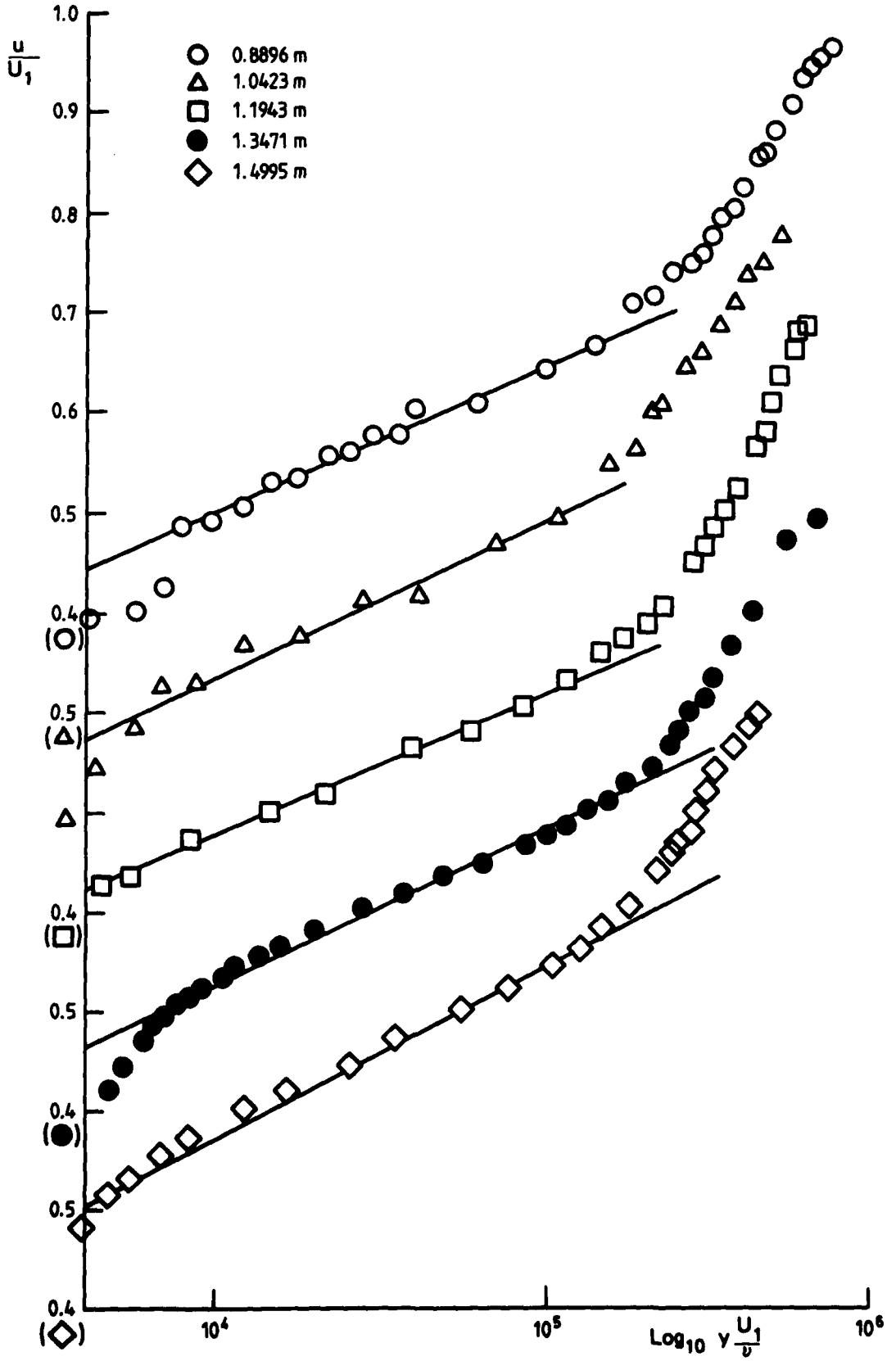

FIG. A1 (Concluded)

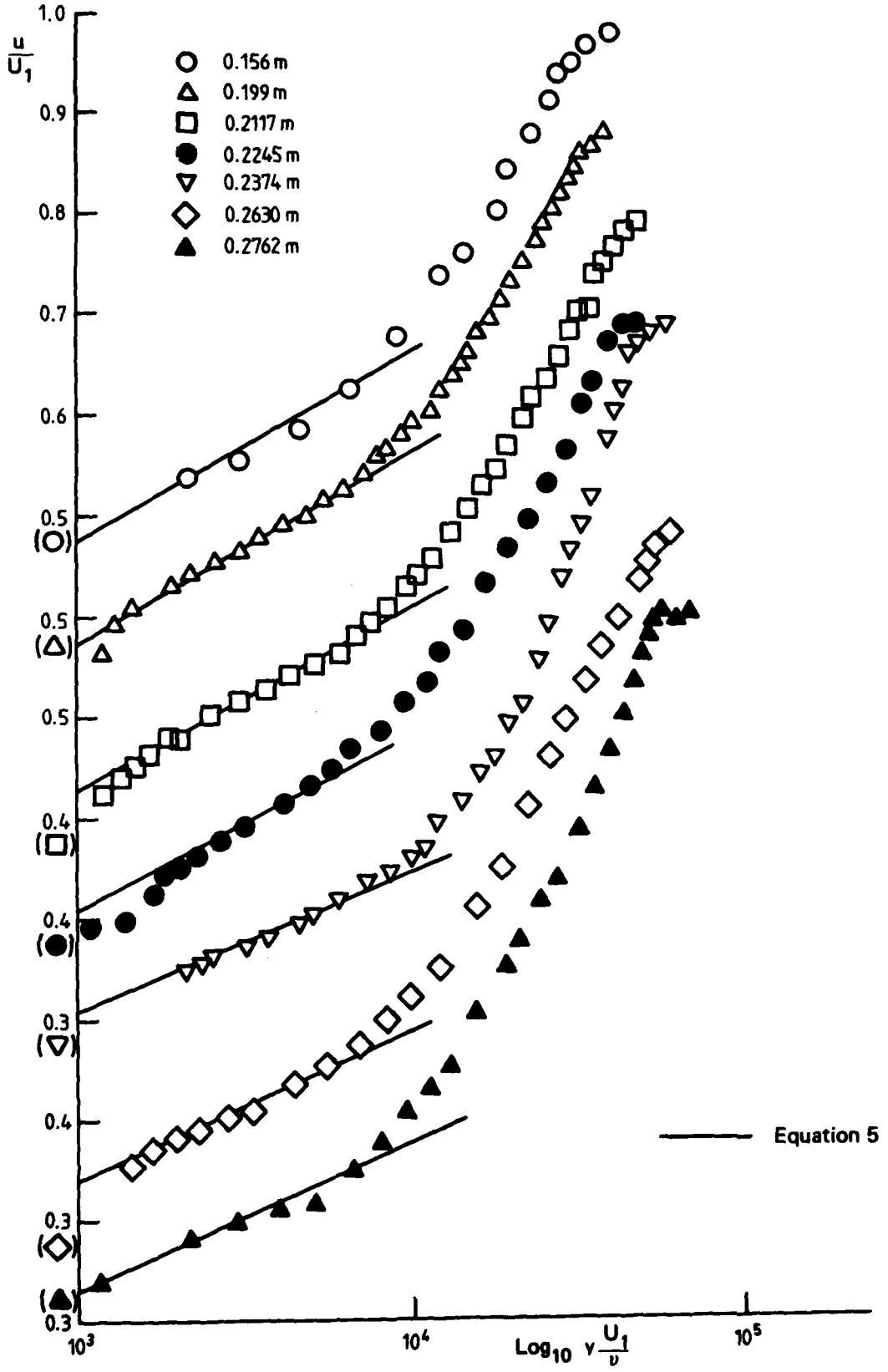

FIG. A2 – SERIES L

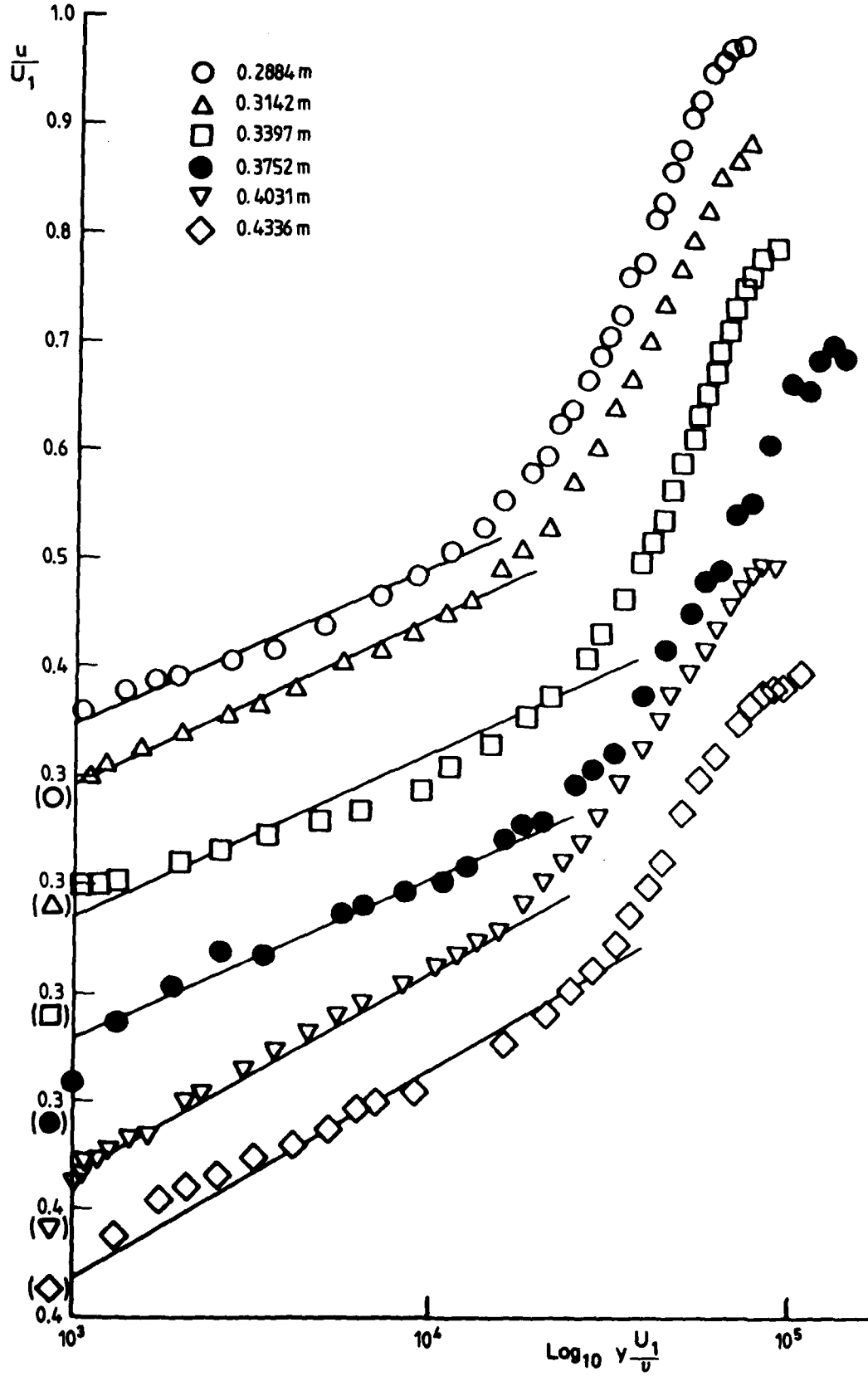

FIG. A2 (Continued)

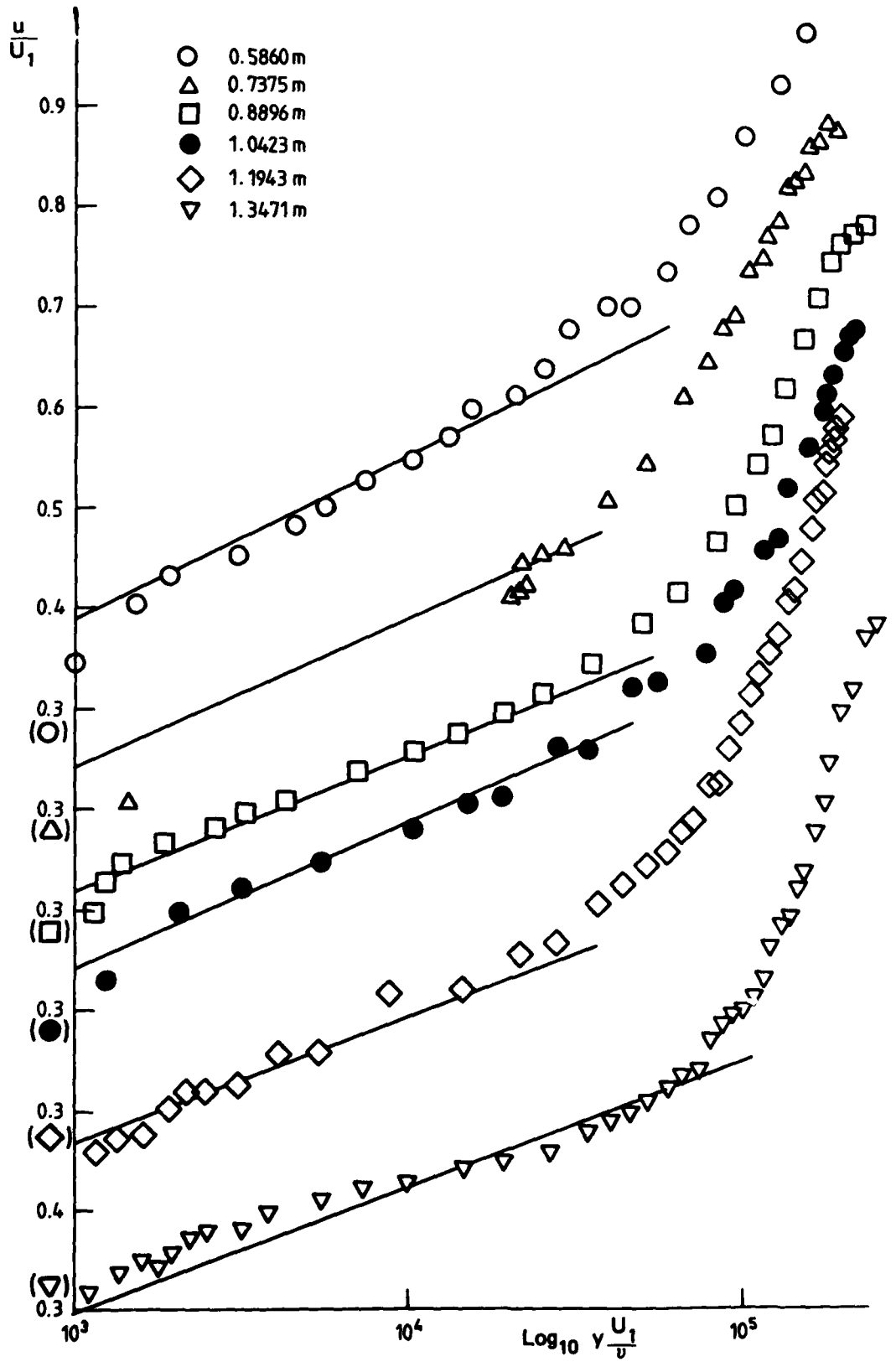

FIG. A2 (Concluded)

DISTRIBUTION

AUSTRALIA

DEPARTMENT OF DEFENCE

Central Office

Chief Defence Scientist
Deputy Chief Defence Scientist
Superintendent, Science and Technology Programmes } 1 copy
Controller, Projects and Analytical Studies
Defence Science Representative (U.K.) (Doc. Data sheet only)
Counsellor, Defence Science (U.S.A.) (Doc. Data sheet only)
Defence Central Library
Document Exchange Centre, D.I.S.B. (17 copies)
Joint Intelligence Organisation
Librarian H Block, Victoria Barracks, Melbourne
Director General—Army Development (NSO) (4 copies)

Aeronautical Research Laboratories

Director
Library
Superintendent—Mechanical Engineering
Divisional File—Mechanical Engineering
Author: W. H. Schofield (5 copies)
S. A. Fisher
D. A. Frith
P. B. Atkins
B. D. Fairlie
A. P. Cox

Materials Research Laboratories

Director/Library

Defence Research Centre

Library
Mr M. L. Robinson

RAN Research Laboratory

Library

Army Office

Army Scientific Adviser
Engineering Development Establishment, Library

Air Force Office

Air Force Scientific Adviser
Aircraft Research & Development Unit
Scientific Flight Group
Library

UNIVERSITIES AND COLLEGES

Adelaide	Professor of Mechanical Engineering
Flinders	Library

Latrobe	Library
Melbourne	Engineering Library
	Professor P. N. Joubert
	Dr A. E. Perry
Monash	Hargrave Library
	Professor W. H. Melbourne
Newcastle	Library
	Professor R. A. Antonia
New England	Library
Sydney	Engineering Library
	Professor G. A. Bird
	Professor R. I. Tanner
	Professor R. Bilger
N.S.W.	Professor R. A. A. Bryant, Mechanical Engineering
Queensland	Professor K. Bullock
Tasmania	Dr G. Walker

CANADA

NRC

Aeronautical & Mechanical Engineering Library
Division of Mechanical Engineering, Director

Universities and Colleges

Toronto	Institute for Aerospace Studies

FRANCE

ONERA, Library

GERMANY

Fachinformationzser·rum: Energie, Physic, Mathematik GMBH

Universities and Colleges

Universitat Karlsruhe	Professor Rodi
Universitat Erlangen	Dr G. Scheuerer

INDIA

Defence Ministry, Aero Development Establishment, Library
Gas Turbine Research Establishment, Director
Hindustan Aeronautics Ltd, Library
National Aeronautical Laboratory, Information Centre

ISRAEL

Technion-Israel Institute of Technology
Professor J. Singer

JAPAN

Institute of Space and Aeronautical Science, Library

NETHERLANDS

National Aerospace Laboratory (NLR), Library

NEW ZEALAND

RNZAF, Vice Consul (Defence Liason)

SWEDEN

Aeronautical Research Institute, Library
Swedish National Defense Research Institute (FOA)

SWITZERLAND

Dr Escudier, BBC Limited, Baden
Dr A. Gyr, E.T.H., Zurich

UNITED KINGDOM

CAARC, Secretary (NPL)
Royal Aircraft Establishment—Farnborough
Dr L. F. East
Royal Aircraft Establishment—Bedford
Mr E. L. Goldsmith (2 copies)
Dr W. G. Sawyer
National Gas Turbine Establishment
Director, Pyestock North
National Physical Laboratory, Library
National Engineering Laboratory, Library
British Library, Lending Division
CAARC Co-ordinator, Structures
Aircraft Research Association, Library
GEC Gas Turbines Ltd, Managing Director
Rolls-Royce Ltd, Aero Division Bristol, Library
British Aerospace
Kingston-upon-Thames, Library
Hatfield-Chester Division, Library

Universities and Colleges

Cambridge	Library, Engineering Department
	Dr A. A. Townsend, Mathematics Department
Manchester	Professor N. Johannesen, Fluid Mechanics
Nottingham	Science Library
Southampton	Library
Liverpool	Fluid Mechanics Division, Dr J. C. Gibbings
Caulfield Institute of Technology	Library
Imperial College	Aeronautics Library
	Professor P. Bradshaw
Salford	Professor J. L. Livesey

UNITED STATES OF AMERICA

NASA Scientific and Technical Information Facility
NASA Langly Research Center, Dr D. Bushnell
Applied Mechanics Reviews
Boeing Co.
Mr R. Watson
Mr J. C. McMillan
United Technologies Corporation, Library
Lockheed Georgia
McDonnell Aircraft Company, Library
David Taylor Naval Ship R & D Center, Dr P. S. Granville

Universities and Colleges

Princeton	Professor S. Bogdonoff
	Professor G. L. Mellor, Mechanics
	Dr A. J. Smits
California Institute of Technology	Professor D. Coles
Arizona State	Professor E. Logan
Southern Methodist	Dr R. L. Simpson
Pensylvania State	Dr. G. S. Settles

Spares (50 copies)
TOTAL (177 copies)

Department of Defence Support

DOCUMENT CONTROL DATA

1. a. AR No.	1. b. Establishment No.	2. Document Date	3. Task No.
AR-002-950	ARL-MECH-ENG-REPORT-161	April, 1983	DST 82/050

4. Title	5. Security	6. No. Pages
INTERACTION OF A NORMAL SHOCK WAVE AND A TURBULENT BOUNDARY LAYER WITH A POST SHOCK ADVERSE PRESSURE GRADIENT	a. document: Unclassified b. title: U. c. abstract: U.	26 7. No. Refs: 38

8. Author(s)	9. Downgrading Instructions
W. H. SCHOFIELD	—

10. Corporate Author and Address	11. Authority (*as appropriate*)
Aeronautical Research Laboratories, G.P.O. Box 4331, Melbourne, Vic. 3001.	a. Sponsor c. Downgrading b. Security d. Approval

12. Secondary Distribution (*of this document*)

Approved for public release

Overseas enquirers outside stated limitations should be referred through ASDIS, Defence Information Services Branch, Department of Defence, Campbell Park, CANBERRA, ACT, 2601.

13. a. This document may be ANNOUNCED in catalogues and awareness services available to . . .

No limitation

13. b. Citation for other purposes (*i.e. casual announcement*) may be ~~(select)~~ unrestricted ~~(or) as for 13 a.~~

14. Descriptors		15. COSATI Group
Turbulent boundary layer	Shock waves	2004
Turbulent flow	Models	
Turbulence		
Boundary layer separation	Jet engines	
Air intakes	Engine installation	

16. Abstract

An experimental study has been made of the development of a turbulent boundary layer after an interaction with a normal shock wave (strong enough to cause a local separation) in a strong adverse pressure gradient. This type of flow occurs in air breathing engine components (e.g. supersonic intakes, transonic compressor stages and supersonic diffusers), is poorly understood and cannot be satisfactorily predicted. The measurements, made in a closed duct, extended well downstream of the shock wave interaction. Detailed results for the flow are presented and used to support two major conclusions. Firstly it is shown that the post shock adverse pressure gradient has a large effect on boundary layer development through the interaction and downstream of it. Consequently existing results for interactions without a post shock pressure gradient should not be used as a model for practical flows which typically have strong pressure gradients applied downstream of the shock wave. The second conclusion was that the shock wave in a rectangular

This page is to be used to record information which is required by the Establishment for its own use but which will not be added to the DISTIS data base unless specifically requested.

16. Abstract (*Contd*

duct produced a pronounced stabilising effect on the downstream flow. Surface flow visualization suggests that this stabilization is achieved by streamwise vortices shed into the flow from the separated region formed by the shock wave. The implication of this result to nominally two dimensional flow situations and to flows with weak interactions without local separations, is discussed.

17. Imprint

Aeronautical Research Laboratories, Melbourne

18. Document Series and Number	19. Cost Code	20. Type of Report and Period Covered
Mechanical Engineering Report 161	42 7405	—

21. Computer Programs Used

22. Establishment File Ref(s)

—

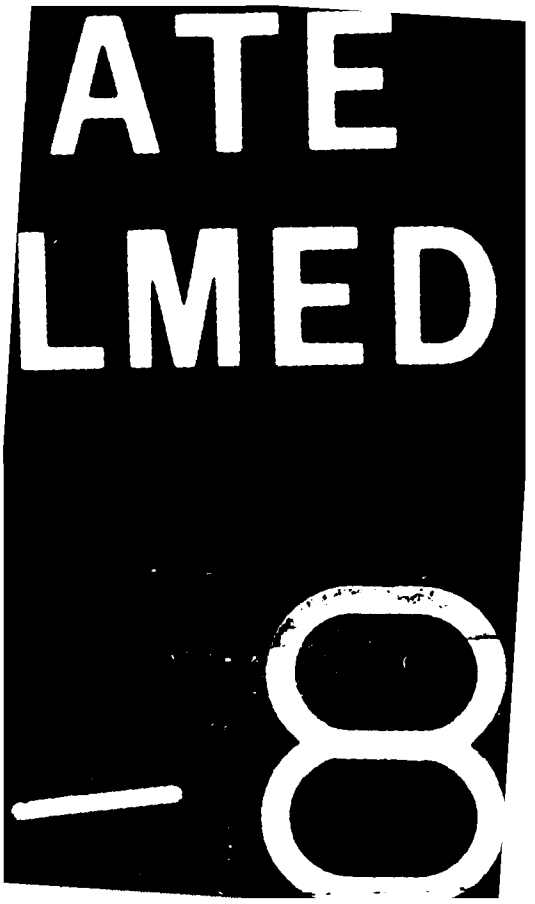
ATE
LMED
8